

# 1 Large-scale drivers of Caucasus climate variability in meteorological 2 records and Mt Elbrus ice cores

3  
4 Anna Kozachek<sup>1,2,3</sup>, Vladimir Mikhalenko<sup>2</sup>, Valérie Masson-Delmotte<sup>3</sup>, Alexey Ekaykin<sup>1,4</sup>, Patrick  
5 Ginot<sup>5,6</sup>, Stanislav Kutuzov<sup>2</sup>, Michel Legrand<sup>5</sup>, Vladimir Lipenkov<sup>1</sup>, Susanne Preunkert<sup>5</sup>

6  
7 1. Climate and Environmental Research Laboratory, Arctic and Antarctic Research Institute, St Petersburg, 199397, Russia

8 2. Institute of Geography, Russian Academy of Sciences, Moscow, 119017, Russia

9 3. Laboratoire des Sciences du Climat et de l'Environnement, CEA/CNRS/UVSQ/IPSL, Gif-sur-Yvette, 91191, France

10 4. Institute of Earth Sciences, St Petersburg State University, St Petersburg, 199178, Russia

11 5. Laboratoire de Glaciologie et Géophysique de l'Environnement, CNRS/UGA, Grenoble, 38400, France

12 6. Observatoire des Sciences de l'Univers de Grenoble, IRD/UGA/CNRS, Grenoble, 38400, France

13  
14 *Correspondence to:* Anna Kozachek (kozachek@aari.ru)

## 15 16 **Abstract**

17  
18 A 181.8 m ice core was recovered from a borehole drilled into bedrock on the western plateau of Mt Elbrus (43°20'53.9'' N,  
19 42°25'36.0'' E; 5115 m a.s.l.) in the Caucasus, Russia, in 2009 (Mikhalenko et al., 2015). Here, we report on the results of  
20 the water stable isotope composition from this ice core with additional data from the shallow cores. The distinct seasonal  
21 cycle of the isotopic composition allows dating by annual layer counting. Dating has been performed for the upper 126 m of  
22 the deep core combined with 20 m from the shallow cores. The whole record covers 100 years, from 2013 back to 1914. Due  
23 to the high accumulation rate (1380 mm w.e. per year) and limited melting we obtained isotopic composition and  
24 accumulation rate records with seasonal resolution. These values were compared with available meteorological data from 13  
25 weather stations in the region, and also with atmosphere circulation indices, back-trajectory calculations and GNIP data in  
26 order to decipher the drivers of accumulation and ice core isotopic composition in the Caucasus region. In the warm season  
27 (May-October) the isotopic composition depends on local temperatures, but the correlation is not persistent over time, while  
28 in the cold season (November–April), atmospheric circulation is the predominant driver of the ice core's isotopic  
29 composition. The snow accumulation rate correlates well with the precipitation rate in the region all year round, which made  
30 it possible to reconstruct and expand the precipitation record at the Caucasus highlands from 1914 till 1966 when reliable  
31 meteorological observations of precipitation at high elevation began.

## 32 33 **1 Introduction**

34  
35 Large-scale modes of variability such as the NAO (North Atlantic Oscillation) are known to influence European climate  
36 variability (see review in Panagiotopoulos et al., 2002). However, most studies of large-scale drivers of European climate

37 change have been focused on low elevation instrumental records from weather stations, and there is very limited information  
38 about climate variability at high altitudes, and about differences in climate variability and trends at different elevations  
39 (EDW research group, 2015). Such differences were calculated in many mountain regions (EDW research group, 2015),  
40 except for the Caucasus, due to the lack of high elevation instrumental observations in this region.

41 The Caucasus is located southwards of the East European Plain. It is a high mountain region, with typical elevations of 3200-  
42 3500 m a.s.l., and with the highest point reaching 5642 m for Elbrus. The Main Caucasus Ridge acts as a barrier between  
43 subtropical and temperate mid-latitude climates, as observed for other high mountain regions such as the Himalaya. As in  
44 other mountain regions, there is a lack of high elevation meteorological records in the Caucasus. Moreover, existing records  
45 are relatively short: for example, reliable Caucasus precipitation measurements only started in 1966. Improved spatio-  
46 temporal coverage is required to investigate internal variability, to explore trends and spatial differences, and to evaluate the  
47 skills of atmospheric models providing atmospheric analysis products where no meteorological data are assimilated.

48 Measurements of the stable isotope composition of water, and annual accumulation rates in mid to high latitude ice cores are  
49 widely used proxies to estimate past temperature and precipitation rate changes. In many high mountain regions such as the  
50 Caucasus, and for elevations situated above the tree line, ice core data provides the only source of detailed information to  
51 document past climate changes, complementing punctual information retrieved from changes in glacier extent and recent  
52 glacier mass balance. For example, a study of the water stable isotope composition of several ice cores obtained in the Alps  
53 was recently conducted by Mariani et al. (2014) and the same research in Alaska was performed by Tsushima et al. (2015).

54 The authors explored the links between the ice cores' isotopic composition, local climate and large-scale circulation patterns.  
55 They found that in mountain regions, the isotopic composition of the ice cores was governed both by local meteorological  
56 conditions and by regional and global factors. These studies discussed the complexity of interpreting ice core records from  
57 high-altitude glaciers due to the potential bias from post-depositional processes and frequent changes in the origin of  
58 moisture sources. For instance, even in areas without any seasonal melt, accumulation is the net effect of precipitation,  
59 sublimation, and wind erosion processes, and may significantly differ from precipitation. Water stable isotope records are in  
60 mid to high latitudes physically related to condensation temperature through distillation processes (Dansgaard, 1964), but the  
61 climate signal is archived through the snowfall deposition and post-deposition processes. One important artefact lies in the  
62 intermittency of precipitation, and the covariance between condensation temperature and precipitation, which may bias the  
63 climate record towards one season, or towards one particular weather regime, challenging an interpretation in terms of  
64 annual mean temperature (Persson et al., 2011). Moreover, water stable isotopes are integrated tracers of all phase changes  
65 occurring from evaporation to mountain condensation, and are also affected by non-local processes related to evaporation  
66 characteristics, or shifts in initial moisture sources. Such processes have the potential to alter the validity of an interpretation  
67 of the proxy record in terms of local, annual mean, or precipitation-weighted temperature. In some region, isotopic records  
68 are more related to hydrological cycles, recycling, rainout (Aemisegger et al., 2014). Finally, the condensation temperature  
69 may also strongly differ from surface air temperature; depending on elevation shifts in e.g. planetary boundary layer or  
70 convective activity (see Ekaykin and Lipenkov, 2009 for a review). While these processes make the interpretation of ice core

71 records complex, they do open the possibility that the ice core proxy record may be in fact more sensitive to large-scale  
72 climate variability than punctual precipitation amounts. For instance, Casado et al (2014) have evidenced a strong fingerprint  
73 of the NAO in water stable isotope records from central Western Europe and Greenland, either in long instrumental records  
74 based on precipitation sampling, in seasonal ice core records, or in atmospheric models including water stable isotopes. The  
75 connection of Greenland ice cores' isotopic composition with the atmospheric circulation patterns was studied by Vinther et  
76 al. (2003 and 2010). The strong influence of the NAO pattern on the Greenland ice cores isotopic composition has been  
77 discovered and the possibility to use the ice cores data for the reconstruction of the past NAO changes was suggested  
78 (Vinther et al., 2003). The authors also revealed the importance of the study of the seasonally resolved ice cores records  
79 rather than annual records as there are different factors governing formation of the isotopic composition of precipitation in  
80 warm and in cold seasons (Vinther et al., 2010).

81 We will now briefly review earlier studies performed on climate variability in the Caucasus area, which have already  
82 explored the relationships between regional climate, glacier expansion, and large-scale modes of variability: the NAO (North  
83 Atlantic Oscillation), AO (Arctic Oscillation), and NCP (North Sea–Caspian Pattern). For example, Shahgedanova et al.  
84 (2005) monitored the mass balance of the Djankuat glacier, situated at an altitude between 2700 and 3900 m a.s.l. While no  
85 significant correlation was identified between accumulation rate and the winter NAO index, the years of high accumulation  
86 systematically occurred during winters with a very negative NAO index. Brunetti et al. (2011) explored the influence of the  
87 NCP mode on climate in Europe and around the Mediterranean region. They evidenced a negative correlation coefficient of -  
88 0.50 between temperature in the Caucasus and the NCP index. Baldini et al. (2008) investigated records of precipitation  
89 isotopic composition in Europe from the IAEA/GNIP stations, extrapolating a significant negative correlation between  
90 winter precipitation  $\delta^{18}\text{O}$  in the Caucasus region and the NAO index ( $R = -0.50$ ). Casado et al (2013) studied the influence  
91 of precipitation intermittency on the relationships between precipitation  $\delta^{18}\text{O}$ , temperature, and the NAO. The influence of  
92 the NAO index on European climate and precipitation  $\delta^{18}\text{O}$  appeared more prominent in winter than in summer (Comas-Bru  
93 et al., 2016).

94 Here, we take advantage of the new Elbrus deep ice cores (Mikhalevko et al., 2015), and produce the first analysis of water  
95 stable isotope and accumulation records. Section 2 introduces the data and methods, with a description of the ice core  
96 analyses and age scale, an overview of regional meteorological information, and the source of information for indices of  
97 modes of variability. Section 3 presents the results of the comparison and statistical analyses of the relationships between  
98 regional climate parameters (temperature and precipitation), Elbrus ice core records, and modes of variability. In section 4,  
99 we summarize our key findings and the next steps envisaged to strengthen the climatic interpretation of the Caucasus ice  
100 core records.

## 101 **2 Data and methods**

### 102 **2.1 Ice core data**

105

106 **2.1.1 Drilling site and drilling campaigns**

107

108 Here, we report on results from the new, deepest ice core from Mt Elbrus, in comparison with results from shallow ice cores.  
109 Deep drilling was performed on the Western Plateau (43°20'53.9" N, 42°25'36.0" E; 5115 m a.s.l.) of Mt Elbrus (fig. 1) in  
110 September 2009, allowing recovery of a 181.8 m long ice core, down to bedrock. The drilling site and the drilling operations  
111 are thoroughly described in Mikhalenko et al. (2015).

112 In order to update the ice core records towards the present-day, and enable a comparison of the measurements with local  
113 meteorological monitoring data, surface drilling operations were repeated at the same place in 2012 (11.5 m long) and in  
114 2013 (20.5 m long). Results are also compared here with previously published isotopic composition data measured along the  
115 22 m shallow ice core drilled at the same place in 2004 which covered the period from 1998 till 2004. (Mikhalenko et al,  
116 2005).

117 In 2014, drilling operations were also successful at the Maili Plateau (Mt Kazbek), at the altitude of 4500 m a.s.l. in 200 km  
118 eastwards from Elbrus (fig. 1), delivering a 20-m ice core. The Kazbek core is shown for purposes of comparison only. A  
119 detailed description of it will be published elsewhere.

120

121 **2.1.2 Sampling process and sampling resolution**

122

123 For the upper and the lower parts of the deep core (0-106 m and 158-181.8 m) and for the shallow firn cores drilled in 2012  
124 and 2013, sampling was performed using classical cutting-melting procedures. For the other depth intervals, melted samples  
125 were extracted from the continuous flow analysis system of LGGE (Grenoble, France), automatically sub-sampled, frozen  
126 and stored in vials for subsequent isotopic analysis. The description of the CFA system will be published elsewhere.

127 The sampling resolution was 15 cm for the upper 16 m of the deep core (see the sketch of the sampling resolution in fig. 2c).  
128 It was then increased to 5 cm in order to achieve better resolution, from 16 to 70 m depth and in the bottom part of the core  
129 (158-182 m depth). To ensure 15-20 samples per year, the sampling resolution was increased to 4 cm in the depth range from  
130 70 to 106 m, similar to the sampling resolution of the CFA system (3.7 cm).

131 Samples from the shallow cores drilled in 2012 and 2013 were cut with a resolution of 10 and 5 cm, respectively.

132

133 **2.1.3 Isotopic measurements**

134

135 The methods for the isotopic measurements have been partially discussed in (Mikhalenko et al., 2015). Water stable isotope  
136 ratios ( $\delta^{18}\text{O}$  and  $\delta\text{D}$ ) were measured at the Climate and Environmental Research Laboratory (CERL) at the Arctic and  
137 Antarctic Research Institute (St Petersburg, Russia), using a Picarro L2120-i analyzer. Each sample was measured once.  
138 Sequences of measurements included the injection of 5 samples, followed by the injection of an internal laboratory standard

139 with an isotopic value close to that of the samples. We also repeated the measurements of about 10% of all the samples in  
140 order to calculate the analytical precision: 0.06‰ for  $\delta^{18}\text{O}$  and 0.30‰ for  $\delta\text{D}$ . The depth profile of  $\delta^{18}\text{O}$  (Mikhalenko et al.,  
141 2015; Kozachek et al., 2015) and of the deuterium excess ( $d = \delta\text{D} - 8 * \delta^{18}\text{O}$ ) are shown in fig. 2.

142 Moreover, 600 samples from the depth interval from 23 to 35 m were measured in the Laboratory of Isotope Hydrology of  
143 the IAEA (Vienna, Austria). The two records are highly correlated ( $r=0.99$ ,  $p < 0.05$ ) for both isotopes (Figure S2b) with a  
144 systematic offset of 0.2 ‰ for  $\delta^{18}\text{O}$  and 1 ‰ for  $\delta\text{D}$ . The records of the second order parameter deuterium excess are also  
145 significantly correlated ( $r=0.65$ ,  $p < 0.05$ ) without any specific trend or systematic offset. This inter-laboratory comparison  
146 demonstrates the high quality of the isotopic measurements performed in CERL.

147 We also stress the close overlap of the upper part of the profiles of the water stable isotope records versus depth from the  
148 different cores drilled in 2009, 2012 and 2013 (Fig. S2a). Based on this close agreement within the different shallow firn  
149 cores, we decided to calculate a stack record for the period from 1914 till 2013 which is used for dating hereafter.

150 In the depth interval from 100 to 106 m depth, we also have an overlap of samples obtained with classical cutting method  
151 and CFA method described above, without any significant difference (Fig. S2c), again allowing us to combine the two  
152 records into one stack record.

153

#### 154 **2.1.4 Dating**

155

156 The chronology is based on the identification of annual layers. These are prominent in  $\delta^{18}\text{O}$  with the average seasonal  
157 amplitude of 20 ‰. For annual mean values we calculated averages of  $\delta^{18}\text{O}$  from one minimum of this parameter to another  
158 one as well as from one maximum to another. As we found no significant differences between the records obtained with two  
159 ways of year allocation we used minimum to minimum dating as a more common method. We compared annual layer  
160 counting performed independently using the seasonal cycles in the isotopic composition and the ammonium concentration.  
161 The discrepancy between two independent chronologies is 2 years at a depth of 126 m. We used the dating based on the  
162 isotopic composition data in this paper. This dating is also best fit for the correlation analysis with the meteorological data.  
163 For the estimation of the dating uncertainties we used the absolute age markers. These markers are the tritium peak in 1963  
164 and the sulfate peak in 1912 which corresponds to the Katmai eruption (Mikhalenko et al., 2015). The comparison of  
165 different dating methods on age control points shows that the overall error of our timescale at these two depth levels does not  
166 exceed  $\pm 2$  years which means that independent dating uncertainties should compensate each other at this points

167 Hereafter, we focus our analysis on one hundred years, from 1914 till 2013, which corresponds to the total of 140 m of the  
168 ice thickness studied here (the 15 m covered by the shallow cores plus the 126 m covered by the deep ice core. This period  
169 has been chosen because of the relatively small dating uncertainty ( $\pm 2$  years) and the availability of other records such as  
170 local meteorological observations. In the bottom part of the core the cycles in the isotopic composition are less prominent  
171 and dating becomes less reliable leading to a significant increase in uncertainty. The isotopic composition of that part of the

172 core will be discussed elsewhere. In meteorological data we used average values from January to December of each year for  
173 the comparison with annual means of ice cores parameter.

174 For warm and cold seasons allocation we used a method adapted slightly from (Vinther et al., 2010). The original method  
175 requires ascribing of an equal accumulation rate for the warm and cold season of each year. Basically we used the same  
176 approach as there is an obvious seasonal cycle of  $\delta^{18}\text{O}$  which is coherent with the seasonal cycle of temperature in the region.  
177 We therefore assume that the maximum value of  $\delta^{18}\text{O}$  in the annual cycle corresponds to July and the minimum value  
178 corresponds to January and put the border so that these extreme values are in the middle of a season. However, there were  
179 several situations (six for the whole ice core record) when this approach could potentially lead to assign minimum values to  
180 summer and maximum to winter. In order to avoid this problem we used the middle point between minimum and maximum  
181 as a border between seasons in such cases. We also used ammonium concentration as an independent marker, using criteria  
182 described on (Mikhaleiko et al., 2015). For equivocal situations, we also used additional data: melt layers and dust layers  
183 (used to identify the warm season) (Kutuzov et al., 2013) as well as succinic acid concentration data that also have seasonal  
184 variations (Mikhaleiko et al., 2015).

185 Figure 3 illustrates the identification of seasons using the isotopic composition seasonal cycle. In the meteorological data we  
186 used period from November to April for the cold season and May to October for the warm season.

187 There some gaps in the isotopic composition data that came from technical problems during the drilling operations and the  
188 process of analysis. The drilling problems are described in (Mikhaleiko et al., 2015). The biggest gap appears at the depth of  
189 31.3 and 32.1 m. A piece of the core was lost during the drilling operations. This part is covered by the bottom part of the  
190 2004 core where the sampling resolution was 50 cm. It is evident that two seasons (one warm and one cold) are partially  
191 missing. We did not use these values for the correlation analysis because of the large uncertainty of the seasonal values  
192 calculations in this case. In case of a missing sample we considered its isotopic value to be the average between the two  
193 neighboring samples. For a detailed description of the raw isotopic data and annual layers allocation for the upper 106 m of  
194 the core, please refer to Mikhaleiko et al. (2015). Mean annual and seasonal values of  $\delta^{18}\text{O}$  and  $d$  obtained as a result of the  
195 dating are shown in fig. 5 and 6 respectively.

196 The annual accumulation rate is calculated as the thickness of the seasonal layer, multiplied by the layer density using the  
197 density profile from Mikhaleiko et al. (2015), and corrected for layer thinning using the Nye model (Nye, 1963; Dansgaard  
198 and Johnsen, 1969), with the following parameters: accumulation rate 1.583 m of ice equivalent, pore close-off depth = 55 m  
199 (Mikhaleiko et al., 2015).

200

### 201 **2.1.5 Diffusion of stable isotopes**

202

203 We calculated the potential influence of diffusion on the stable isotopes record according to (Johnsen, 2000) model. We used  
204 the following parameters for the calculation: Our calculation showed that the seasonal amplitude of  $\delta^{18}\text{O}$  variations could be  
205 10-20% less because of the diffusion (Mikhaleiko et al., 2015). If it was the case we would observe a decreasing of  $\delta^{18}\text{O}$

206 maxima and increasing of minima with depth. Moreover we would find a positive correlation between layer thickness and a  
207 seasonal amplitude of  $\delta^{18}\text{O}$ . These features have not been found in the ice core data. The correlation coefficient between  
208 seasonal amplitude and accumulation rate is -0.10 and is statistically insignificant. There is also no statistically significant  
209 trend in the seasonal amplitude; the seasonal amplitude varies stochastically from 10 to 25 %. The maximum value observed  
210 in 1984 and the minimum in 1925. We therefore consider that the diffusion does not sufficiently influence the isotopic  
211 composition record in the upper 126 m of the ice core. At the bottom part of the core (e.g. at a depth of 180 m) the annual  
212 cycle of  $\delta^{18}\text{O}$  should have an amplitude of 4 ‰ which is detectable but the length of the cycle should be less than 1 cm. As  
213 the  $d$  annual cycle is not prominent we cannot use the method based on the discrepancy between the  $\delta^{18}\text{O}$  and  $d$  cycles.  
214 Thus, for obtaining climatic information from the bottom part of the core, a very high sampling resolution is required.  
215

## 216 **2.2 Meteorological data**

217  
218 We used the daily meteorological data (precipitation rate and mean daily temperature) from several weather stations around  
219 the drilling site (see map in Fig. 1 and Table 1) for comparison with the ice core data. We also investigated records of  
220 precipitation isotopic composition based on monthly sampling, performed at three stations to the south of the Caucasus  
221 within the WMO-IAEA Global Network of Isotopes in Precipitation (GNIP) program (Table 1).

222 For comparison we used the NCEP/NCAR reanalysis temperature data (Kalnay et al., 1996) for the 500 mbar level which  
223 corresponds to the drilling site altitude. Two different models were used to calculate back trajectories: FLEXPART (Forster  
224 et al., 2007, Stohl et al., 2009), HYSPLIT (Draxler, 1999, Stein et al., 2015, Rolph, 2016). The LMDZiso model was used to  
225 estimate the precipitation isotopic composition at the drilling site (Risi et al., 2010).  
226

## 227 **2.3. Circulation indices**

228 Circulation of the atmosphere sufficiently influences isotopic composition of the ice cores (Casado et al., 2013 and  
229 references therein). Atmospheric circulation is quantitatively characterized by circulation indices. In this research we used  
230 three indices: NAO, AO, and NCP that are widely used to characterize European climate (Jones et al., 2003, Thompson and  
231 Wallace, 2001, Brunetti et al., 2011 and references therein). Time span and references for the indices are presented in table 1.  
232 NAO (North-Atlantic Oscillation) characterizes the type of circulation in Europe, strength of Azores maximum and Icelandic  
233 minimum. The positive values of the NAO index correspond to the lower than usual value of the atmospheric pressure in  
234 Iceland and the higher than usual value of atmospheric pressure at Azores. The negative index corresponds to the less  
235 prominent centres of action in the Northern Hemisphere. Usually this index is calculated as a difference of atmospheric  
236 pressure measured at Reykjavik and Lisbon, Ponta Delgada or Gibraltar. Here we used data from (Vinther et al., 2003 and  
237 <https://crudata.uea.ac.uk/~timo/datapages/naoi.htm>) that were calculated using data from Gibraltar station. The negative  
238 NAO leads to an increase in the precipitation rate in Southern Europe, while a positive NAO leads to an increase in the  
239 precipitation rate in Northern Europe (Hurrell, 1995, Jones et al., 2003, Vinther et al., 2003).

240 The Arctic Oscillation index (AO) is also a characteristic of the Northern Hemisphere circulation. It is used to analyze  
241 climatic variability with periods longer than 10 years. It is calculated as EOF of 500 hPa surface. Negative values correspond  
242 to high pressure at the Pole and the cooling of Europe, while positive values correspond to low pressure at the Pole and the  
243 drying of the Mediterranean (Thompson and Wallace, 2001). We used AO data from NOAA  
244 (<http://www.cpc.ncep.noaa.gov/products/precip/CWlink/>).

245 The NCP (North-Sea Caspian Pattern) index is less widely used, though it was proved that it is convenient to use it in  
246 Mediterranean climate studies (Kutiel et al., 1997; Brunetti et al., 2011). The index is calculated as a normalized difference  
247 of geopotential heights between the Caspian and Northern seas. Positive values correspond to stronger meridional circulation  
248 in Europe and lower summer temperatures, while negative values reflect the strengthening of zonal circulation and higher  
249 summer temperatures in Europe (Brunetti et al., 2011). We used NCP data from NOAA  
250 (<http://www.cpc.ncep.noaa.gov/products/precip/CWlink/>).

251

## 252 **3 Results**

253

### 254 **3.1 Regional climate**

255

256 The main peculiarity of the drilling site is its location on the border between subtropical and temperate climatic zones  
257 (Volodicheva, 2004). Back-trajectory calculations show that the drilling site is characterized by remarkable seasonal  
258 differences in the locations of moisture sources. In winter, the origin of air masses varies from the Mediterranean to the  
259 North Atlantic. In summer, local moisture sources from the surrounding continents or from the Black Sea are predominant  
260 (see fig. S1 for examples).

261 Meteorological data depict large regional variations in the seasonal cycle of precipitation. To the south of the Caucasus, there  
262 is no distinct seasonal cycle (Fig. 4a), showing the climatology for the Klukhorskyy Pereval station. In fact, the Klukhorskyy  
263 Pereval station is situated north of the Main ridge, but in terms of the seasonal cycle of precipitation it undoubtedly belongs  
264 to the southern group. However, we are nevertheless using this station as an example because of the uninterrupted record of  
265 temperature and precipitation for the 1966-1990 period. By contrast, the north of the Caucasus is marked by a distinct  
266 seasonality in precipitation amounts, which are maximum in summer and minimum in winter (Fig. 4b), showing the  
267 climatology for the Mineralnye Vody station. More examples of the Caucasus weather stations climatologies are given in  
268 (Mikhaleiko et al., 2015). Moreover, the annual precipitation rate to the south of the Caucasus is much higher than to the  
269 north. For example, the typical annual precipitation rate to the north of the Caucasus at an altitude close to sea level is 500  
270 mm per year, while to the south of the Caucasus at the same altitude it is about 1500 mm. The amount of precipitation in the  
271 region is affected by the altitude and the distance from the sea shore.

272 The seasonal changes of temperature appear uniform throughout the region surrounding the Caucasus, with the warmest  
273 conditions observed in summer and the coldest observed in winter. The seasonal amplitude depends on the distance from the



274 sea and the mean annual temperature depends on the altitude. The average regional lapse rate was calculated using the  
275 available meteorological data. We used the data from all the stations for the calculation. The lapse rate is lowest in  
276 December-February (2.3°C per 1000 m) and highest (5.2 °C per 1000 m) in June-August (Fig. S3).

277 Based on the lapse rate, we calculated the temperature at the drilling site taking into account its seasonal variability shown  
278 on the fig. S3. This record was used for the estimation of the  $\delta^{18}\text{O}$ -temperature relationship. For the comparison with the ice  
279 core data we used the dataset of the normalized temperature data. Normalized temperature time series were calculated for  
280 each station for each season or for the whole year, and results were then averaged (fig. 8). For precipitation data, available in  
281 this region since 1966, we show all the data (fig. S4), while in the calculations we used data from Klukhorskii Pereval  
282 station as an example of stations without a seasonal cycle, and from Mineralnye Vody station as an example of those with a  
283 prominent cycle. More examples of annual variations of temperature and precipitation at the Caucasus meteorological  
284 stations can be found in (Shahgedanova et al., 2014) and (Tielidze, 2016). At our drilling site, an automatic weather station  
285 (AWS) provided in situ measurements for the period from August 2007 till January 2008. The day to day variations of  
286 temperature at low elevation weather stations and at the AWS are coherent for the whole period of the AWS work  
287 (Mikhaleiko et al., 2015).

288 We also compared the data from meteorological stations with the NCEP reanalysis (Kalnay et al., 1996) outputs (not shown)  
289 for the 500 mbar level. Despite the difference in absolute values on a daily scale when compared with the AWS data (the  
290 difference is random and varies from -1 to 1 °C), the observed regional data and reanalysis data have the same month to  
291 month variability. The maximum daily mean temperature at the drilling site according to the reanalysis data was -1.3°C for  
292 the whole dataset. The temperature in the glacier at 10m depth, which corresponds to the annual mean temperature at the  
293 drilling altitude, is -17°C (Mikhaleiko et al., 2015), the annual mean temperature at the drilling altitude from the NCEP  
294 reanalysis is -14 °C, and the same value calculated from meteorological observations and corrected for the lapse rate is -11  
295 °C.

296 We then investigated long-term trends in the meteorological records. Mean annual temperatures show a significant increase  
297 during the last two decades. We also observe higher than average values of mean decadal temperature in 1930-1940. And the  
298 beginning of the observations in the region, i.e. the period from 1881 till 1900, was as cold as the 1990s. It is evident that the  
299 last 20 years in the warm season were the warmest for the whole observation period (fig. 8), while in the cold season the  
300 recent warming is not unprecedented. For example, cold seasons in the 1960s – 1970s were even warmer (fig. 8). Multi-  
301 decadal patterns of temperature variations also differ in the late 19<sup>th</sup> century, where negative anomalies are identified in cold  
302 season temperature (Fig. 8) but not in warm season temperature (Fig. 8). On the other hand in cold season temperatures we  
303 can observe lower temperatures at the end of the 19<sup>th</sup> century that can be due to the impact of the volcanic eruptions (Stoffel  
304 et al., 2015). We also noted the high temperature values in the 1910s - 1920s that are not completely understood. We did not  
305 find any trends in the precipitation rate for any of the groups of stations (fig. S4).

306 A significant anti-correlation is observed between temperature and the NAO index, both in the cold and warm seasons  
307 (Table 2, the information about the time series used for the correlation analysis can be found in Table 1). Stronger anti-

308 correlations are identified between temperature and the NCP index, especially in the cold season, as also reported by Brunetti  
309 et al. (2011). Relationships with indices of large scale modes of variability are systematically weaker for precipitation, with  
310 contradictory results for the south/north Caucasus stack; they appear significant for the NCP in both seasons (Table 2).  
311 GNIP data are only available at low elevation stations. They show a rather uniform distribution of the isotopic composition  
312 of precipitation in the region during summer, as well as a gradual depletion of  $\delta^{18}\text{O}$  at higher altitudes in winter.  
313 GNIP records are too short and intermittent (one-two years with gaps) to investigate the variability and relationships with the  
314 local temperature on an interannual scale. We therefore restrict discussion of GNIP data to seasonal variations. The  $\delta^{18}\text{O}$  and  
315  $\delta\text{D}$  in precipitation have a distinct seasonal cycle with maximum values observed in the warm season (JJA) and minimum  
316 values observed in the cold season (DJF). As an example we show the seasonal cycle of  $\delta^{18}\text{O}$  and  $d$  for Bakuriani station in  
317 2009 (fig. 7). This station is the only one in the region for which the whole uninterrupted dataset for one annual cycle is  
318 available. The seasonal amplitude of  $\delta^{18}\text{O}$  is about 17 ‰. The slope between  $\delta^{18}\text{O}$  and temperature is 0.32 ‰/°C. The  $d$   
319 variations show no seasonal cycle varying randomly between 10 ‰ and 25 ‰. We found no significant correlation between  
320  $\delta^{18}\text{O}$  and  $d$ .

321 Climate variability as a driver for glacier variations in the Caucasus has recently been explored by several authors.  
322 Elizbarashvili et al. (2013) found the increased frequency of extremely hot months during the 20th century, especially over  
323 Eastern Georgia, whereas the number of extremely cold months decreased faster in the Eastern than in the Western region. In  
324 addition, the highest rates for positive trends of annual mean air temperature can be observed in the Caucasus Mountains.  
325 Shahgedanova et al. (2014) evidenced significant glacier recession at the northern slopes of the Caucasus, consistent with  
326 increasing air temperature of the ablation season. They report that the most recent decade (2001-2010) was 0.7–0.8 °C  
327 warmer than in 1960-1986 at Terskol and Klukhorskiy Pereval stations (see Table 1 for information on stations). However,  
328 the warmest decade for JJA was 1951-1960 (Shahgedanova et al., 2014). Tielidze (2016) reports a recent increase in the  
329 annual mean temperatures at different elevations in the Georgian Caucasus. The region experienced glacier area loss over the  
330 20<sup>th</sup> century at an average annual rate of 0.4% with a higher rate in eastern Caucasus than in the central and western sections.  
331 The analysis of temperature and radiation regime of glaciers at the ablation period has been performed at Elbrus vicinities  
332 recently (Toropov et al., 2016). The authors prove that the observed waning of glaciers cannot be explained by increase of  
333 temperature during the ablation period because of an increase in precipitation during the accumulation period. They  
334 concluded that the main driver of glacier retreat is the increase of the solar radiation balance for 4% for the 2001-2010 period  
335 which corresponds to the increase of ablation for 140 mm per ablation season (Toropov et al., 2016).

### 336 337 **3.2 Ice core records**

338  
339 The comparison of the four cores obtained at the Western Plateau of Elbrus shows similar variations during overlap periods  
340 (see Fig. 2S). We therefore calculate a stack record for each season, based on the average value of individual ice cores for the

341 overlapping seasons. The inter-core disagreement is almost negligible (fig. 2S) and can be explained by different sampling  
342 resolution.

343 We note that the shallow ice core from the Maili plateau of Kazbek shows the same mean values of  $\delta^{18}\text{O}$  as the Elbrus ice  
344 cores during their overlap period. This is a result of a mutual compensation of  $\delta^{18}\text{O}$  increase due to lower elevation position  
345 (Kazbek drilling site is 500 m lower) and of  $\delta^{18}\text{O}$  decrease because of continentality effect (Kazbek is 200 km further from  
346 the sea). We calculated continental gradient and lapse rate for  $\delta^{18}\text{O}$  using the data from the GNIP stations in the region that  
347 are situated at the lower elevations. The lapse rate is  $-0.25\text{‰}/100\text{ m}$  and continental gradient is  $-0.85\text{‰}/100\text{ km}$ . The mean  
348 value of  $\delta^{18}\text{O}$  for Kazbek ice core should be  $1.25\text{‰}$  more positive because of elevation difference and  $1.7\text{‰}$  more negative  
349 due to continentality factor.

350 The inter-annual variability in isotopic composition is about twice larger in the cold season than in the warm season for  $\delta^{18}\text{O}$ .  
351 Different patterns of inter-annual to multi-decadal variations appear in the instrumental temperature data (see section 3.1)  
352 and ice core  $\delta^{18}\text{O}$  records (Fig 5) emerge for the cold versus the warm season.

353 The  $\delta\text{D}$  and  $\delta^{18}\text{O}$  values are highly correlated ( $r = 0.99$ ) on a sample to sample scale so hereafter we use the  $\delta^{18}\text{O}$  information  
354 for the dating and comparison with the other parameters. The slope between  $\delta^{18}\text{O}$  and  $\delta\text{D}$  is 8.03 on sample to sample scale  
355 and 7.9 on a seasonal scale without any significant difference between the two seasons.

356 No significant (R squared is insignificant at  $p < 0.05$ ) centennial trend is identified in cold / warm season  $\delta^{18}\text{O}$ , nor in the  
357 cold/warm season accumulation rate or deuterium excess. We observe large variations in  $\delta^{18}\text{O}$  with high and variable values  
358 in the early 20<sup>th</sup> century, lower and more stable values in the 1940s-1960s, and a step increase in the 1970s with another  
359 level. These variations are coherent in both seasons as well as in annual means but are not reflected in the meteorological  
360 observations. There is also an increase of  $\delta^{18}\text{O}$  in the last two decades in both seasons in regard to the 1970s-1980s values  
361 but the absolute values of  $\delta^{18}\text{O}$  are close to the multiannual seasonal averages (Table 3). The highest decadal values of  $\delta^{18}\text{O}$   
362 in both seasons are observed in 1912-1920. While a recent warming trend is observed in the regional meteorological data (in  
363 warm season), it is much less prominent in the ice core  $\delta^{18}\text{O}$  record, suggesting a divergence between  $\delta^{18}\text{O}$  and regional  
364 temperature. One of the possible explanations for this feature is the post-depositional change of the isotopic composition.  
365 But we do not expect a significant influence of the post-depositional processes because of the high snow accumulation rate.  
366 The highest  $\delta^{18}\text{O}$  values for a single year correspond to the warm periods of 1984 and 1928, two years for which no unusual  
367 feature is identified from meteorological observations. The highest snow accumulation rate (fig. 9) is observed in both  
368 seasons of 2010, in coherence with the meteorological precipitation data, and also corresponding with a record low winter  
369 NAO index.

370 Our deuterium excess record (fig. 2b) does not depict any robust seasonal variation. Moreover, the distribution of deuterium  
371 excess as a function of  $\delta^{18}\text{O}$  does not display any clear structure. By contrast, deuterium excess is weakly positively  
372 correlated with the accumulation rate during the warm season ( $r = 0.31$ ,  $p < 0.05$ ). This finding is consistent with the GNIP  
373 data in the region that show no link between  $\delta^{18}\text{O}$  and deuterium excess. The smoothed values of deuterium excess have  
374 prominent cycles with a period of about 25 years that are synchronous in both seasons (fig. 6). Deuterium excess is highly

375 sensitive to surface humidity, which itself is very different and depends on the arrival of maritime air masses or dry  
376 continental air masses. This may add to the complexity of the deuterium excess signal (Pfahl and Wernli, 2008).

### 377 378 **3.3 Comparison of ice core records with regional meteorological data**

379  
380 We compared the ice core data with the regional meteorological data and the large-scale modes of variability. The result of  
381 the correlation analysis is summarized in Table 4. Multiannual variations of the parameters are shown in fig. 9 for the cold  
382 season and in fig. 10 for the warm season.

383 We found no significant correlation between the ice core  $\delta^{18}\text{O}$  record and regional temperature, neither with the reanalysis  
384 data, nor with the observation data, when using the whole period. A significant correlation ( $r = 0.44$ ,  $p < 0.05$ ) emerges for  
385 warm season data, when calculated for the period since 1984. The slope for this period is 0.6 per mille per  $^{\circ}\text{C}$ . We also  
386 repeated our linear correlation analysis using precipitation weighted temperature, and obtained the same results. The  
387 precipitation weighted temperature was calculated using daily meteorological data. We used data from two stations:  
388 Klukhorskiy Pereval (as a representative of the southern stations) and Mineralnye Vody (as a representative of the northern  
389 stations).

390 Obviously, the above inferences strongly depend on the uncertainties of the timescale used. If one concedes that the error of  
391 the timescale could be significantly greater than  $\pm 2$  year, quite different conclusions may be reached by adjusting the scale of  
392 the  $\delta^{18}\text{O}$  and T records against each other. For instance, by contracting the  $\delta^{18}\text{O}$  record by 8 years with respect to the initial  
393 timescale in Figs 9 and 10, one would find much better correlation between  $\delta^{18}\text{O}$  and temperature, thus reaching the  
394 conclusion that the local temperature is the main driver of the  $\delta^{18}\text{O}$  variability. However, based on various experimental  
395 evidences, as discussed in the dating section, we argue that the timescale developed for the Elbrus ice core is accurate within  
396  $\pm 2$  years. Therefore, the most realistic conclusion of those that can be drawn from the data obtained is that the temperature is  
397 weakly correlated with the  $\delta^{18}\text{O}$ , and that this correlation is unstable in time.

398 We also did not find any statistically significant correlations when compared 3-, 5-, 7-years running means of these  
399 parameters. This result implies that the isotopic composition at Elbrus is controlled by both local and regional factors such as  
400 changes in moisture sources. The possibilities for accurate reconstructions of past temperatures are therefore limited. For  
401 more accurate investigation of the  $\delta^{18}\text{O}$  – temperature relation on-site experiments and subsequent modeling is required.

402 Our results are comparable to those obtained in the Alps by Mariani et al. (2014) for the Fiescherhorn glacier where the  
403 authors found significant though weak correlation between temperature and  $\delta^{18}\text{O}$ . However for the Elbrus ice core this  
404 correlation was found in the warm season only.

405 . Another research performed in the Alps by Bohleber et al. (2013) revealed significant correlation of modified local  
406 temperature and the ice core isotopic composition at decadal scale. The authors also report that there are some periods of  
407 correlation absence. The main finding is that for the periods of less than 25 years the difference between the modified dataset  
408 according to the authors' method and original dataset temperature is crucial but for longer periods the two temperature

409 datasets are close to each other. That conclusion implies that the isotopic composition reflects the local temperature in the  
410 high mountain regions to a limited extent. It seems to be impossible to calculate the modified temperature for the Caucasus  
411 region according to the methods described by Bohleber et al. (2013) because of the relatively short and sparse original  
412 datasets.

413 The seasonal accumulation rate is seasonal layer thickness corrected for densification using the density profile from  
414 Mikhalenko et al. (2015) and for the layer thinning due to glacier flow using the Nye model (Nye, 1963; Dansgaard and  
415 Johnsen, 1969). It is linked to the precipitation rate on the stations situated south of the Caucasus in both seasons ( $r = 0.49$ ),  
416 and even more closely related to precipitation from Klukhorski Pereval station ( $r = 0.63$  for both seasons). We therefore  
417 establish a linear regression model for the period 1966-2013, and use this methodology to reconstruct past precipitation rates  
418 for the Klukhorskiy Pereval station (1914-1965), when meteorological records are not reliable or unavailable. The  
419 reconstructed records are shown on fig. 9 and 10 for the cold and warm seasons respectively. We found no significant trend  
420 in the reconstructed precipitation values. Even so, these results may be useful for validation of regional climate models and  
421 water resource assessment.

422 Calculation of the seasonal cycle of precipitation isotopic composition using the LMDZiso model (Risi et al., 2010) do not  
423 correspond to the results obtained from the ice core in absolute values or in amplitude (Fig. S5). This can be explained by a  
424 complicated relief of the region that strongly influences the isotopic composition, but it is not taken into account in the  
425 model. Also in summer Elbrus is in a local convective precipitation system that is not included in the model.

### 426 427 **3.4 Comparison of ice core records with large-scale modes of variability**

428  
429 We did not find any statistically significant correlations between ice cores data and large scale modes of variability when  
430 using the mean annual values. We present the results of calculations in the table 4. We report a weak though significant  
431 ( $p < 0.05$ ) negative correlation ( $r = -0.18$ ) between the ice core accumulation rate record and NAO in the cold season.  
432 Moreover, the year of extremely high accumulation in both seasons (2010) coincides with an extremely low NAO winter  
433 index. The role of NAO in regional climate had also been evidenced by Shahgedanova et al. (2005) for the mass-balance of  
434 the Djankuat glacier situated in 30 km south-east of Elbrus for the period of 1967-2001. Interestingly, the accumulation  
435 record is related to the variability of regional precipitation, but the latter is not significantly related to the NAO. This may  
436 suggest different influences of large-scale atmospheric circulation on precipitation at lower versus higher elevations.

437 The ice core cold season  $\delta^{18}\text{O}$  record shows a positive correlation with the NAO index ( $r = 0.41$ ), while the NAO index is  
438 negatively correlated with regional temperature ( $r = -0.42$ ). It also contradicts the findings of Baldini et al (2008) who, based  
439 on the GNIP low elevation dataset, extrapolated a negative correlation between the  $\delta^{18}\text{O}$  of precipitation and the NAO in this  
440 region. This finding also suggests different drivers of temperature and  $\delta^{18}\text{O}$  at low and higher elevation. We propose the  
441 following explanation for this correlation. During the positive NAO phase, the predominant moisture source for the  
442 Caucasus precipitation is the Mediterranean. During the negative NAO phase the moisture source is the Atlantic. In the first

443 case the precipitation  $\delta^{18}\text{O}$  preserved in the ice core is higher because of the higher initial sea water isotopic composition  
444 (Gat et al., 1996) and the shorter distillation pathway. The continental recycling of moisture (Eltahir and Bras, 1996) also  
445 influences the water isotopic composition. Due to this process the  $\delta^{18}\text{O}$  values became lower while the  $d$  values increase  
446 (Aemisegger et al., 2014), which is observed in our ice core data. In the opposite situation the initial water isotopic  
447 composition is close to 0 ‰ (Frew et al., 2000) and the distillation pathway is longer which leads to lower values of  
448 precipitation  $\delta^{18}\text{O}$ .

449  
450 We explored the links between the ice core parameters ( $\delta^{18}\text{O}$ , accumulation rate) with the NCP index and found no  
451 significant correlation in winter, or in summer despite the significant correlation between the NCP and local temperature and  
452 precipitation. A possible explanation may be that the NCP pattern only affects low elevation regional climate but not high  
453 elevation climate.

454 No significant correlation was identified between deuterium excess and indices of large scale modes of variability. So far, no  
455 regional or large-scale climate signal could be identified in Elbrus deuterium excess. Further investigations using back  
456 trajectories and diagnoses of moisture source and evaporation characteristics will be needed to explore further the drivers of  
457 this second-order isotopic parameter.

458

#### 459 **4 Conclusion**

460

461 We found no persistent link between ice cores  $\delta^{18}\text{O}$  and temperature on an interannual scale, a common feature emerging  
462 from non-polar ice cores (e.g. Mariani et al., 2014). This finding is not an artifact of high elevation versus low elevation  
463 difference, because the variability of the regional temperature stack used for this comparison is in good agreement with the  
464 variability of the temperature at the drilling site as observed by the local AWS.

465 Our ice core records depict large decadal variations in  $\delta^{18}\text{O}$  with high and variable values in the late 19<sup>th</sup>-early 20<sup>th</sup> centuries,  
466 lower and more stable values in the 1940s-1960s, followed by a step increase in the 1970s. No unusual recent change is  
467 detected in the isotopic composition or in the accumulation rate record, in contrast with the observed warming trend from  
468 regional meteorological data. The accumulation rate appears significantly related to the NAO index coherently with the  
469 earlier results for the Djankuat glacier (Shahgedanova et al. 2005).

470 Based on regional meteorological information and trajectory analyses, the main moisture source is situated not far from the  
471 drilling site in the warm season, and consists of evaporation from the Black Sea and continental evapotranspiration. Changes  
472 in regional temperature during warm season may affect the initial vapour isotopic composition as well as the atmospheric  
473 distillation processes, including convective activity, in a complex way. This may explain the significant albeit non persistent  
474 correlation of summer  $\delta^{18}\text{O}$  and temperature. Cold season moisture sources appear more variable geographically, with  
475 potential contributions from the North Atlantic to the Mediterranean regions. Changes in moisture origin appear to dominate  
476 in regional temperature-driven distillation processes. As a result, the isotopic composition of the ice cores appears mostly

477 related to characteristics of large-scale atmosphere circulation such as the NAO index. The changes in moisture origin also  
478 influence the deuterium excess parameter, which does not have any prominent seasonal variations.  
479 Our data can be used in atmospheric models equipped with water stable isotopes for instance to assess their ability to resolve  
480 NAO-water isotope relationships (Langebroek et al., 2011, Casado et al., 2014). The accumulation rate at the drilling site is  
481 significantly correlated with the precipitation rate and gives information about precipitation variability before the beginning  
482 of meteorological observations.

#### 484 **Acknowledgements**

485  
486 The research was supported by the RFBR grant 14-05-31102. The analytical procedure ensuring a high accuracy of isotope  
487 data obtained at CERL was elaborated with financial support from the Russian Science Foundation, grant 14-27-00030. The  
488 study of dust layers was conducted with the support of RFBR grant 14-05-00137. The measurement of the samples in IAEA  
489 was conducted according to research contracts 16184R0, and 16795. This research work was conducted in the framework of  
490 the International Associated Laboratory (LIA) “Climate and Environments from Ice Archives” 2012–2016, linking several  
491 Russian and French laboratories and institutes. We thank Obbe Tuinenburg and Jean-Louis Bonne for the back trajectory  
492 calculations. We thank Alice Lagnado for improving the English.

#### 494 **References**

- 495 Aemisegger F., Pfahl S., Sodemann H., Lehner I., Seneviratne S.I., Wernli H.: Deuterium excess as a proxy for continental  
496 moisture recycling and plant transpiration, *Atmos. Chem. Phys.*, 14, 4029–4054, doi:10.5194/acp-14-4029-2014, 2014.
- 497 Baldini L.M., McDermott F., Foley A.M., Baldini J.U.L.: Spatial variability in the European winter precipitation  $\delta^{18}\text{O}$ -NAO  
498 relationship: Implications for reconstructing NAO-mode climate variability in the Holocene, *Geophys. Res. Letters*. 35,  
499 doi:10.1029/2007GL032027, L04709, 2008.
- 500 Bohleber P., Wagenbach D., Schoner W., Bohm R.: To what extent do water isotope record from low accumulation Alpine  
501 ice cores reproduce instrumental temperature series? *Tellus B*, 65, 20148, doi:10.3402/tellusb.v65i0.20148, 2013.
- 502 Brunetti M., Kutiel H.: The relevance of the North-Sea Caspian Pattern (NCP) in explaining temperature variability in  
503 Europe and the Mediterranean, *Nat. Hazards Earth Syst. Sci.*, 11, 2881–2888, doi:10.5194/nhess-11-2881-2011, 2011.
- 504 Casado M, Ortega P., Masson-Delmotte V., Risi C., Swingedouw D., Daux V., Genty D., Maignan F., Solomina O., Vinter  
505 B., Viovy N., Yiou P.: Impact of precipitation intermittency on NAO-temperature records, *Clim. Past*, 9, 871-886,  
506 doi:10.5194/cp-9-871-2013, 2013.
- 507 Comas-Bru, L., McDermott, F. and Werner, M. (2016): The effect of the East Atlantic pattern on the precipitation  $\delta^{18}\text{O}$ -  
508 NAO relationship in Europe, *Climate Dynamics*, doi: 10.1007/s00382-015-2950-1
- 509 Dansgaard, W.: Stable isotopes in precipitation, *Tellus*, 16(4), 436–468, 1964

510 Dansgaard, W., Johnsen, S.J.: A flow model and a time scale for the ice core from Camp Century, Greenland, *J. Glaciol.*,  
511 8(53), 215–223, 1969.

512 Draxler, R.R., and Hess G.D.: An overview of the HYSPLIT\_4 modeling system of trajectories, dispersion, and deposition.  
513 *Aust. Meteor. Mag.*, 47, 295-308, 1998.

514 Ekaykin A.A., Lipenkov V.Ya.: Formation of the ice core isotopic composition, *Physics of ice core records II*, ed. T.Hondoh,  
515 *Low Temperature Science*, 68, Hokkaido Univ. Press, Sapporo, 299-314, 2009.

516 Elizbarashvili E.Sh., Elizbarashvili, M.R., Tatishvili, M.E., Elizbarashvili, Sh.E., Elizbarashvili, R.Sh.: Meskhiya Air  
517 temperature trends in Georgia under global warming conditions, *Russ. Meteorol. Hydrol.*, 38, 234–238, 2013.

518 Eltahir E.A.B., Bras R.L.: Precipitation recycling, *Reviews of Geophysics* 34, 3, 367-378, doi: 8755-12 09/96/96 RG-01927,  
519 1996

520 Forster C., Stohl A., Siebert P.: Parametrization of convective transport in a lagrangian particle dispersion model and its  
521 evaluation, *Journ. of Applied Meteorology and Climatology*, 46 (4), 403–422, doi:10.1175/JAM2470.1, 2007.

522 Frew, R., Dennis, P.F., Heywood K.J., Meredith M.P., and Boswell S.M.: The oxygen isotope composition of water masses  
523 in the northern North Atlantic, *Deep Sea Research Part I: Oceanographic Research Papers*, 47, 12, 2265-2286,  
524 doi:10.1016/S0967-0637(00)00023-6, 2000.

525 Gat, J.R., Shemesh, A., Tziperman, E., Hecht, A., Georgopoulos, D., and Basturk, O.: The stable isotope composition of  
526 waters of the eastern Mediterranean Sea, *J. Geophysical Res.*, 101, 3, 6441-6451, doi: 10.1029/95JC02829, 1996.

527 Johnsen S., Clausen H.B., Cuffey K.M., Hoffmann G., Schwander J., Creyts T.: Diffusion of stable isotopes in polar firn and  
528 ice: the isotope effect in firn diffusion, *Physics of Ice Core Records*, Edited by T. Hondoh, Hokkaido University Press,  
529 Sapporo, 121–140, 2000.

530 Kalnay, E., Kanamitsu, M., Kistler, R., Collins, W., Deaven, D., Gandin, L., Iredell, M., Saha, S., White, G., Woollen, J.,  
531 Zhu, Y., Leetmaa, A., Reynolds, B., Chelliah, M., Ebisuzaki, W., Higgins, W., Janowiak, J., Mo, K. C., Ropelewski, C.,  
532 Wang, J., Jenne, R., Joseph, D.: The NCEP/NCAR 40-Year Reanalysis Project, *Bulletin of the American Meteorological*  
533 *Society*, 77, 3, 437-472, doi: 10.1175/1520-0477(1996)077<0437:TNYRP>2.0.CO;2, 1996.

534 Kozachek A.V., Ekaykin A.A., Mikhalenko V.N., Lipenkov V.Y., Kutuzov S.S.: Isotopic composition of ice cores obtained  
535 at the Elbrus Western Plateau, *Ice and Snow*, 55, 4, doi: 10.15356/2076-6734-2015-4-35-49, 35-49, 2015 (in Russian with  
536 English summary)

537 Kutuzov, S., Shahgedanova, M., Mikhalenko, V., Lavrentiev, I, and Kemp, S.: Desert dust deposition on Mt. Elbrus,  
538 Caucasus Mountains, Russia in 2009–2012 as recorded in snow and shallow ice core: high-resolution “provenancing”,  
539 transport patterns, physical properties and soluble ionic composition, *The Cryosphere*, 7(5), 1481–1498, doi:10.5194/tc-7-  
540 1481-2013, 2013.

541 Langebroek, P. M.; Werner, M.; Lohmann, G.: Climate information imprinted in oxygen-isotopic composition of  
542 precipitation in Europe, *Earth and Planetary Science Letters*, 311, 1, 144-154, 10.1016/j.epsl.2011.08.049, 2011.



543 Mariani I., Eichler A., Jenk M., Brönnimann S., Auchmann R., Leuenberger M.C., Schwikowski M.: Temperature and  
544 precipitation signal in two Alpine ice cores over the period 1961–2001, *Clim. Past.* 10, 1093–1108, doi:10.5194/cp-10-1093-  
545 2014, 2014.

546 Mikhailenko V., Sokratov S., Kutuzov S., Ginot P., Legrand M., Preunkert S., Lavrentiev I., Kozachek A., Ekaykin A., Fain  
547 X., Lim S., Schotterer U., Lipenkov V., Toropov P.: Investigation of a deep ice core from the Elbrus western plateau, the  
548 Caucasus, Russia, *The Cryosphere*, 9, 2253–2270, doi:10.5194/tc-9-2253-2015, 2015.

549 Mikhailenko, V.N., Kuruzov, S.S., Lavrentiev, I.I., Kunakhovich, M.G., and Thompson, L.G.: Issledovanie zapadnogo  
550 lednikovogo plato Elbrusa: rezul'taty i perspektivy (Western Elbrus Plateau studies: results and perspectives), *Materialy*  
551 *glyatsiologicheskikh issledovaniy (Data Glaciol. Stud.)*, (99), 185–190, 2005 (in Russian with English summary)

552 Mountain Research Initiative EDW Working Group: Elevation-dependent warming in mountain regions of the world, *Nature*  
553 *Climate Change* 5, 424–430, doi:10.1038/nclimate2563, 2015.

554 Panagiotopoulos F., Shahgedanova M., Steffenson D.B.: A  
555 review of Northern Hemisphere winter time teleconnection patterns, *J. Phys. IV France*, 12, doi: 10.1051/jp4:20020450,  
2002.

556 Persson, A., P. L. Langen, P. Ditlevsen, B. M. Vinther: The influence of precipitation weighting on interannual variability of  
557 stable water isotopes in Greenland, *J. Geophys. Res.*, 116, D20120, doi:10.1029/2010JD015517, 2011.

558 Pfahl S. and Wernli H.: Air parcel trajectory analysis of stable isotopes in water vapor in the eastern Mediterranean, *J.*  
559 *Geophys. Res.*, 113, D20104, doi:10.1029/2008JD009839, 2008.

560 Risi C., Bony S., Vimeux F., Jouzel J.: Water stable isotopes in the LMDZ4 general circulation model: Model evaluation for  
561 present-day and past climate and implications to climatic interpretation of tropical isotopic records, *Journal of Geophysical*  
562 *Research*, 115, D12118, doi:10.1029/2009JD013255, 2010.

563 Rolph, G.D., Real-time Environmental Applications and Display sYstem (READY) Website (<http://ready.arl.noaa.gov>).  
564 NOAA Air Resources Laboratory, Silver Spring, MD, 2016.

565 Shahgedanova M., Nosenko G., Kutuzov S., Rototaeva O., and Khromova T.: Deglaciation of the Caucasus Mountains,  
566 Russia/Georgia, in the 21st century observed with ASTER satellite imagery and aerial photography, *The Cryosphere*, 8(6),  
567 2367–2379, doi:10.5194/tc-8-2367-2014, 2014.

568 Shahgedanova M., Stokes C., Gurney S., Popovnin V.: Interactions between mass balance, atmospheric circulation, and  
569 recent climate change on the Djankuat Glacier, Caucasus Mountains, Russia, *Journ. of Geophys. Research*, 110, D04108,  
570 doi:10.1029/2004JD005213, 2005.

571 Stein, A.F., Draxler, R.R., Rolph, G.D., Stunder, B.J.B., Cohen, M.D., and Ngan, F.: NOAA's HYSPLIT atmospheric  
572 transport and dispersion modeling system, *Bull. Amer. Meteor. Soc.*, 96, 2059–2077, doi: 10.1175/BAMS-D-14-00110.1,  
573 2015.

574 Stoffel M., Khodri M., Corona C., Guillet S., Poulain V., Bekki S., Guiot J., Luckman B.H., Oppenheimer C., Lebas N.,  
575 Beniston M., and Masson-Delmotte V.: Estimates of volcanic-induced cooling in the Northern Hemisphere over the past  
576 1,500 years, *Nature Geoscience* 8, 784–788, doi:10.1038/ngeo2526, 2015.

577 Stohl A., Thompson D.J.: A density correction for lagrangian particle dispersion models, *Boundary Layer Meteorology*, 90  
578 (1), 155–167, doi:10.1023/A:1001741110696, 1999.

579 Tielidze L.G.: Glacier change over the last century, Caucasus Mountains, Georgia, observed from old topographical maps,  
580 Landsat and ASTER satellite imagery, *The Cryosphere*, 10, 713-725, doi:10.5194/tc-10-713-2016, 2016.

581 Toropov P.A., Mikhalenko V.N., Kutuzov S.S., Morozova P.A., Shestakova A.A.: Temperature and radiation regime of  
582 glaciers on slopes of the Mount Elbrus in the ablation period over last 65 years, *Ice and Snow*, 56(1), 5-19,  
583 doi:10.15356/2076-6734-2016-1-5-19, 2016 (In Russian with English summary).

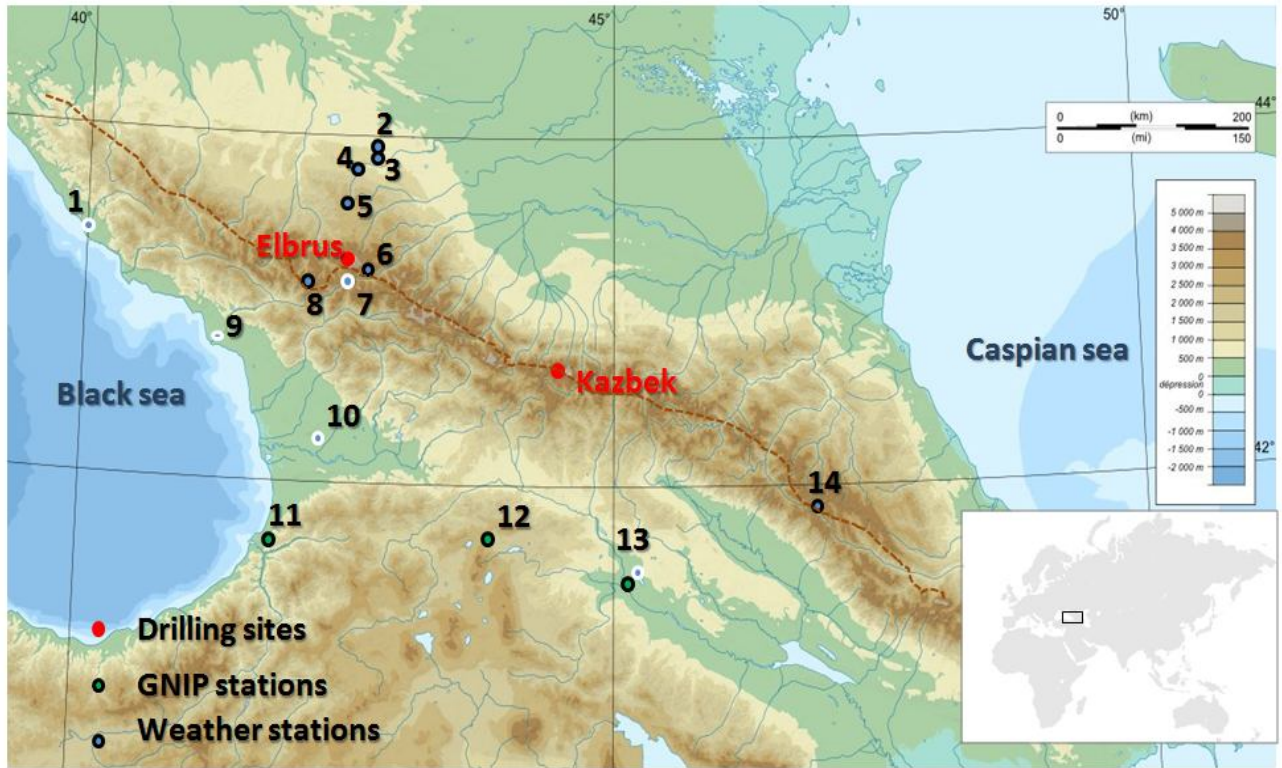
584 Tsushima A., Matoba S., Shiraiwa T., Okamoto S., Sasaki H., Solie D.J., Yoshikawa K.: Reconstruction of recent climate  
585 change in Alaska from the Aurora Peak ice core, central Alaska, *Clim. Past*, 11, 217–226, doi:10.5194/cp-11-217-2015,  
586 2015.

587 Vinther, B. M., S. J. Johnsen, K. K. Andersen, H. B. Clausen, A. W. Hansen: NAO signal recorded in the stable isotopes of  
588 Greenland ice cores, *Geophys. Res. Lett.*, 30(7), 1387, doi:10.1029/2002GL016193, 2003

589 Vinther B.M., Jones P.D., Briffa K.B., Clausen H.B., Andersen K.K., Dahl-Jensen D., Johnsen S.J.: Climatic signals in  
590 multiple highly resolved stable isotopes records from Greenland, *Quat. Sci. Rev.* 29 (3-4), 522-538, 2010

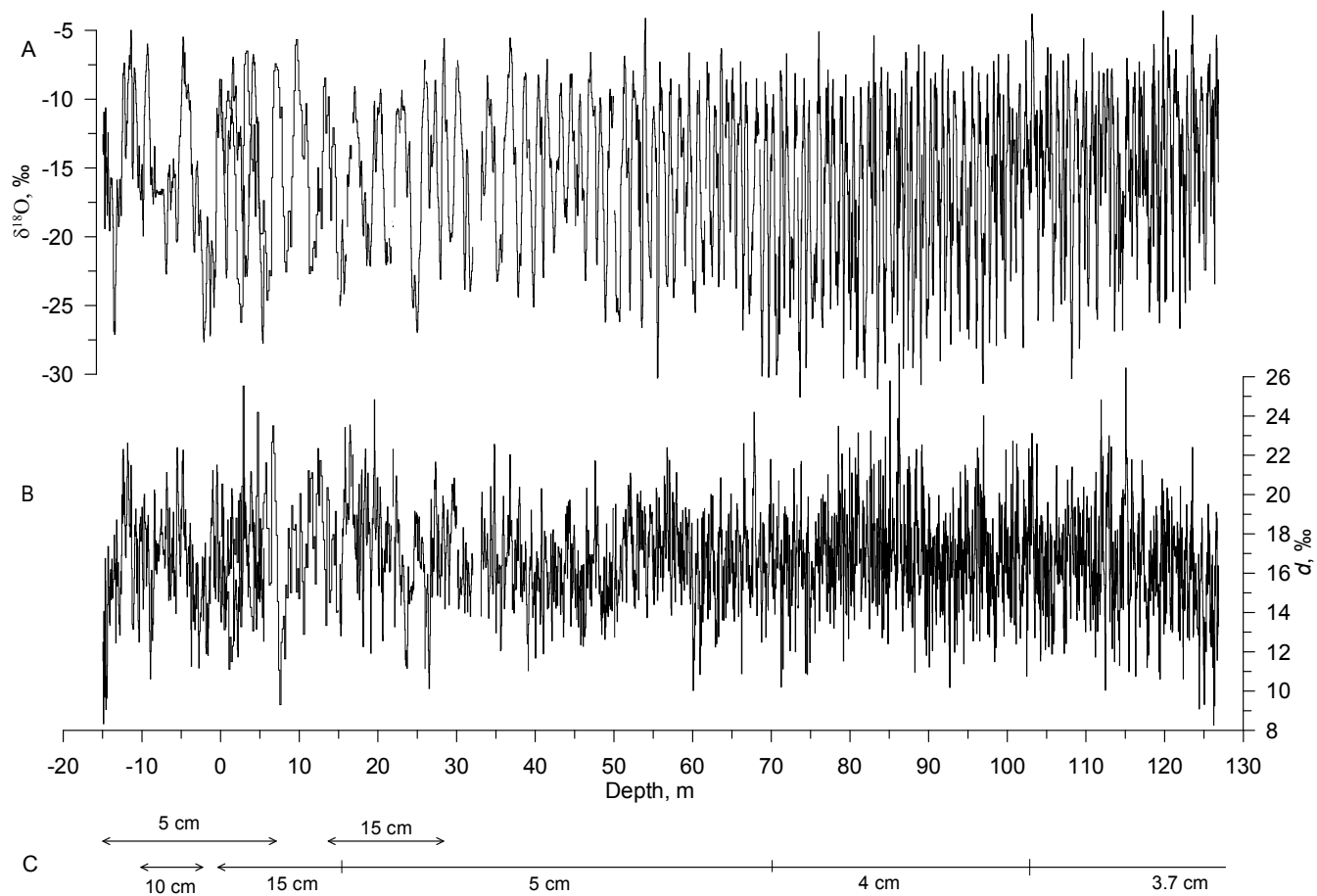
591 Volodicheva, N.: The Caucasus, in: *The Physical geography of Northern Eurasia*, edited by: Shahgedanova, M., Oxford  
592 University Press, Oxford, 350–376, 2002

593 .



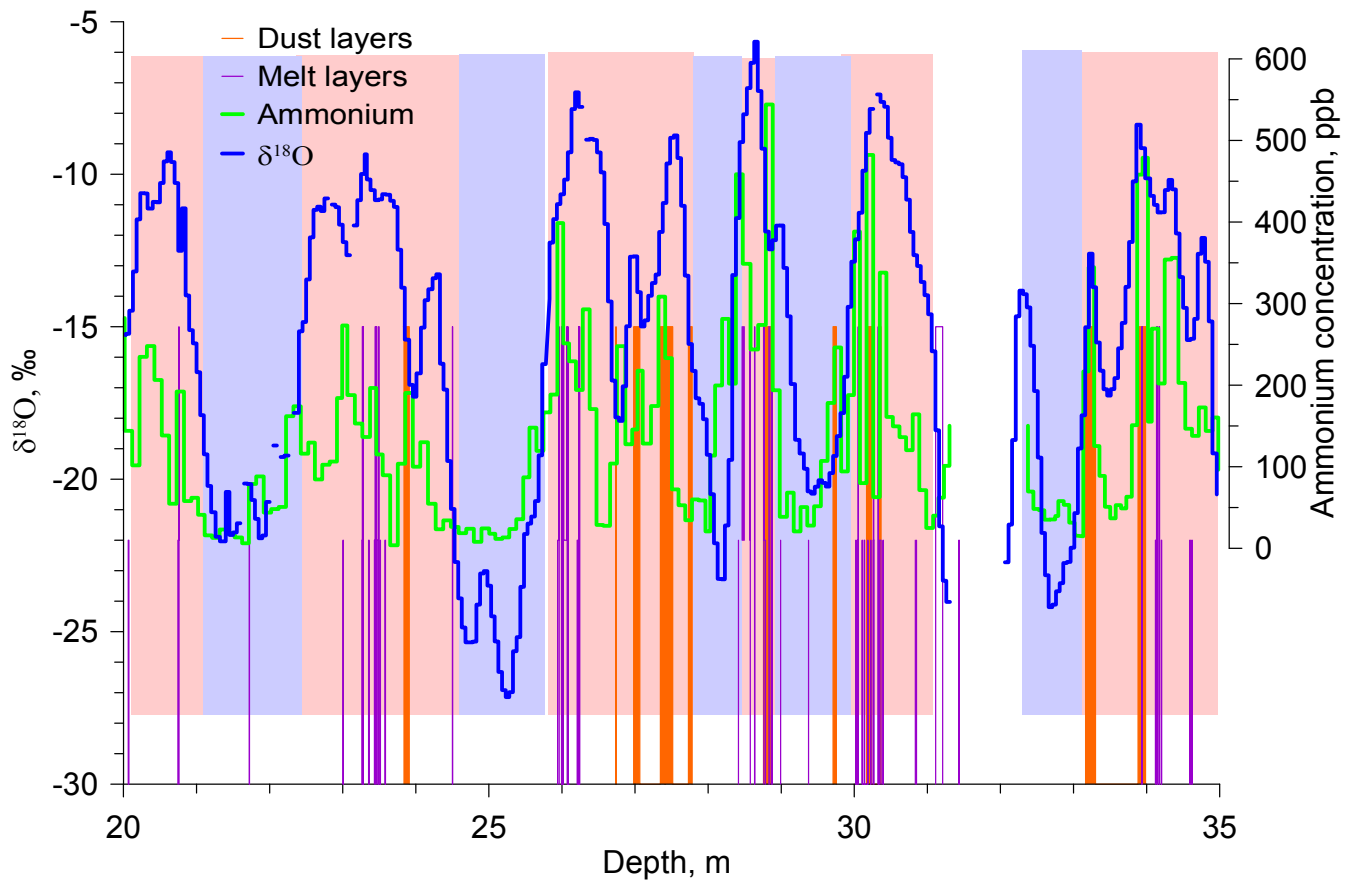
597  
598  
599  
600  
601  
602  
603  
604  
605

Fig. 1: Map showing the region around Elbrus (black rectangle in the world's map in the lower right corner), with shading indicating elevation (m above sea level). Drilling sites are indicated with red filled circles, GNIP stations as green filled circles, and meteorological stations as blue dots. Stations situated to the south of the Main Caucasus Ridge according to the precipitation cycle pattern are shown using a blue dot with white outside circle and the stations situated to the north are displayed with black outside circle (see text for the details). The brown dotted line shows the border between two types of precipitation seasonal cycles. The number of the various stations refers to Table 1 for their detailed description.



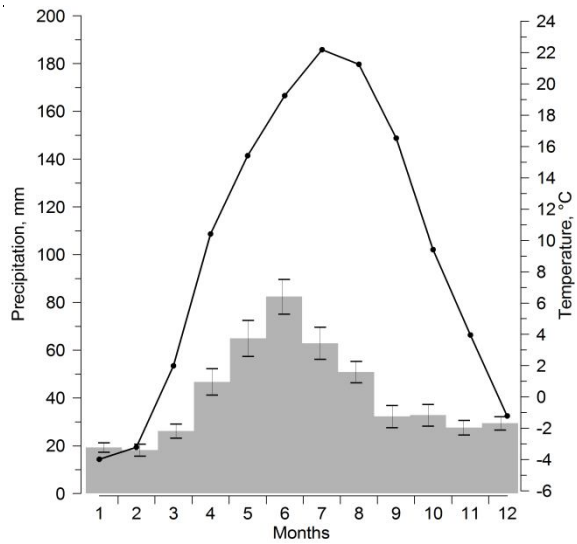
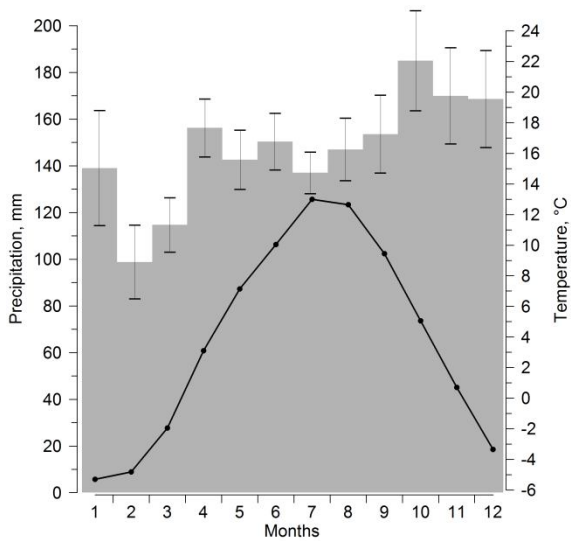
606  
607  
608  
609  
610

**Fig. 2. Vertical profile of  $\delta^{18}\text{O}$  (A), deuterium excess (B), and the number of the ice core as well as sampling resolution (C). 0 m depth corresponds to the surface of 2009.**

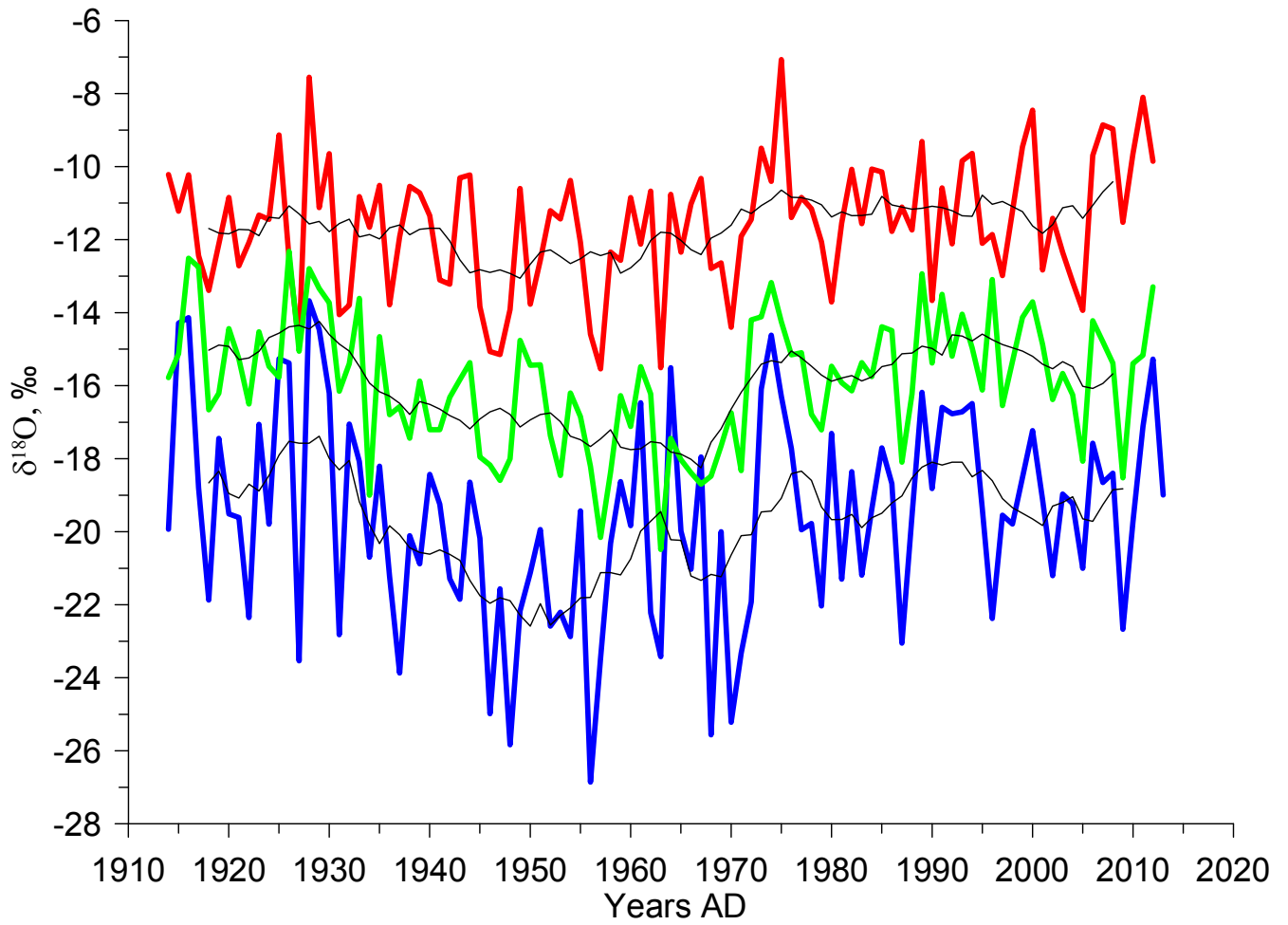


611  
612  
613  
614  
615  
616

Fig. 3: Illustration of the scheme used to identify warm and cold half-years (respectively indicated by the light red and light blue shaded areas) based on the deviation of the mean  $\delta^{18}\text{O}$  values from the long-term average value. The purple lines depict the melt layers observed in the core, dust layers are shown in orange and ammonium concentration graph (Mikhaleiko et al., 2015) is in green.

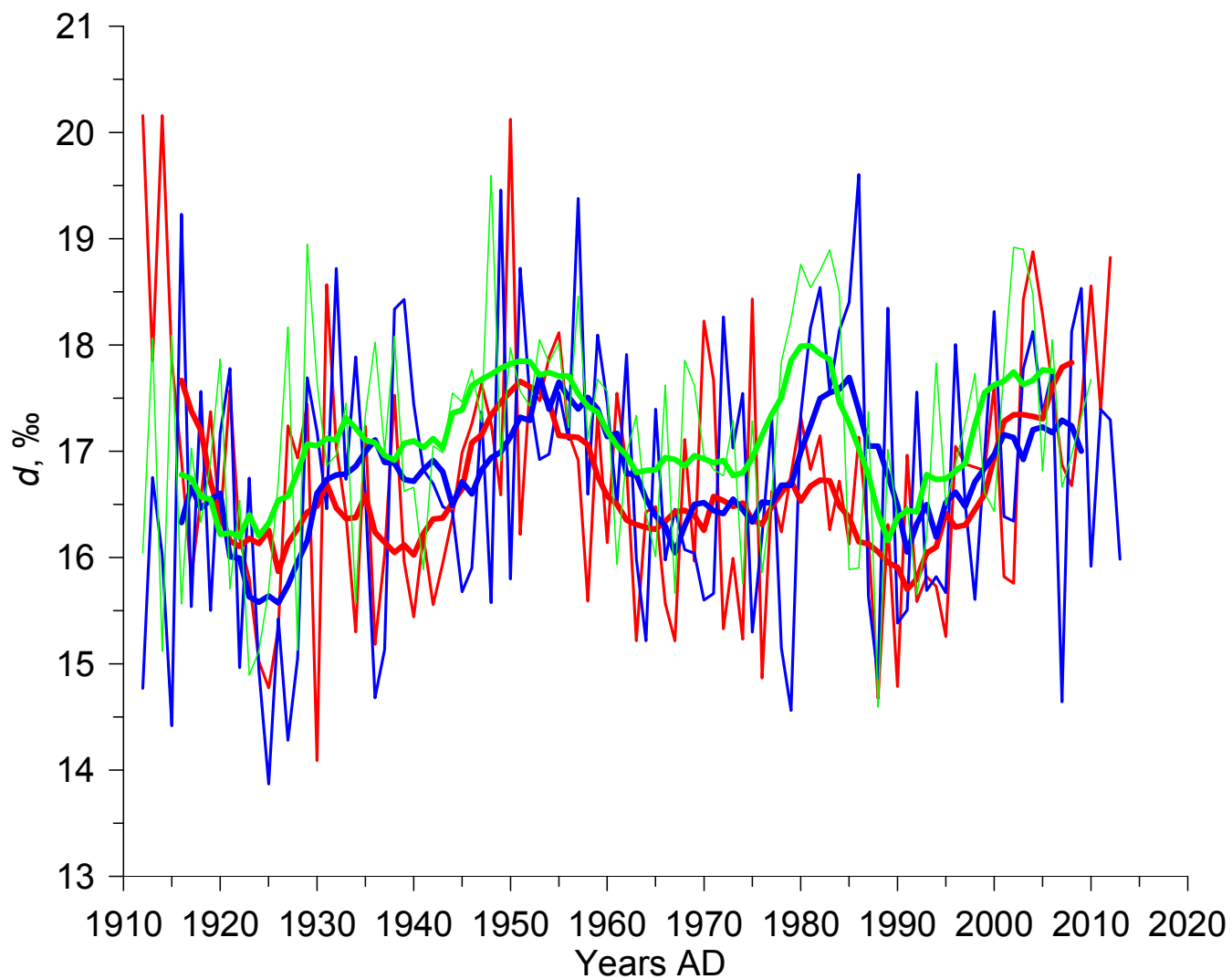


617  
618  
619 **Fig. 4: Average seasonal cycle of temperature (black dots and line) and precipitation (grey bars) calculated over 1966-1990 period,**  
620 **a) for the Klukhorskyy Pereval station (illustrating the lack of a distinct seasonal cycle in precipitation south of the Caucasus) and**  
621 **b) for the Mineralnye Vody station (illustrating the clear seasonal cycle in precipitation seen in stations north of the Caucasus).**  
622 **Error bars (SEM) are shown for the interannual standard deviation of the monthly precipitation rate while the same error bars**  
623 **for the temperature are dimensionless at the scale of the graph.**  
624



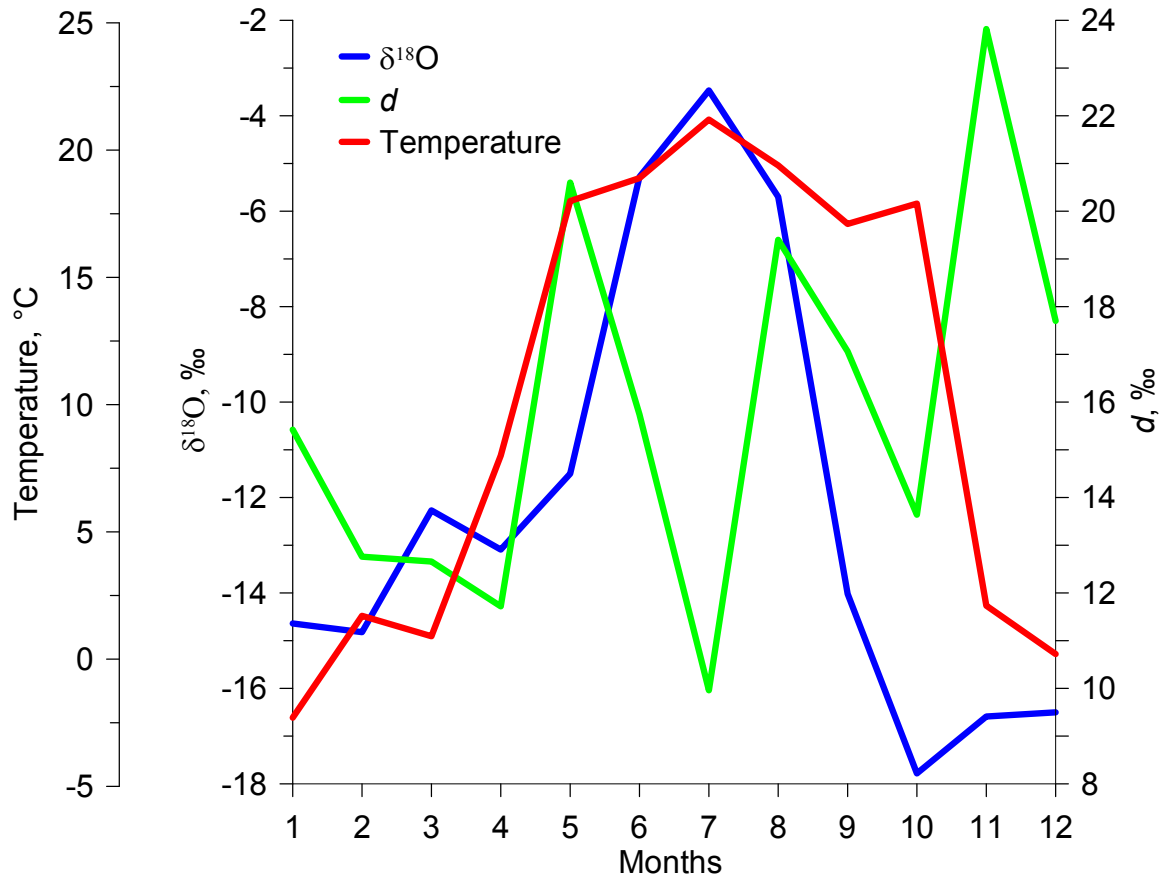
625  
626  
627  
628

**Fig. 5:** Annual variations of  $\delta^{18}\text{O}$  in warm season (red line), in cold season (blue line), and annual means (green line). Thin black lines show 10-year running means of these parameters.



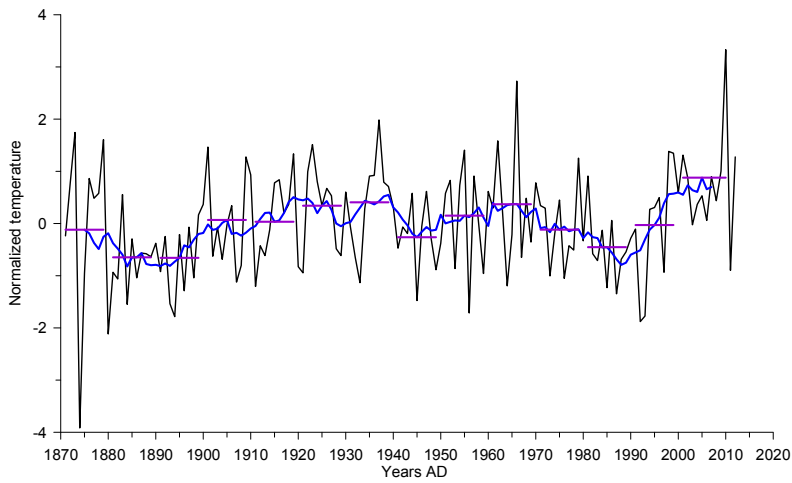
629  
 630 **Fig. 6:** Annual variations of deuterium excess in warm season (red line), in cold season (blue line), and mean annual values (green  
 631 line). Thick lines show the 10-year smoothed values and the thin ones display the raw values.  
 632



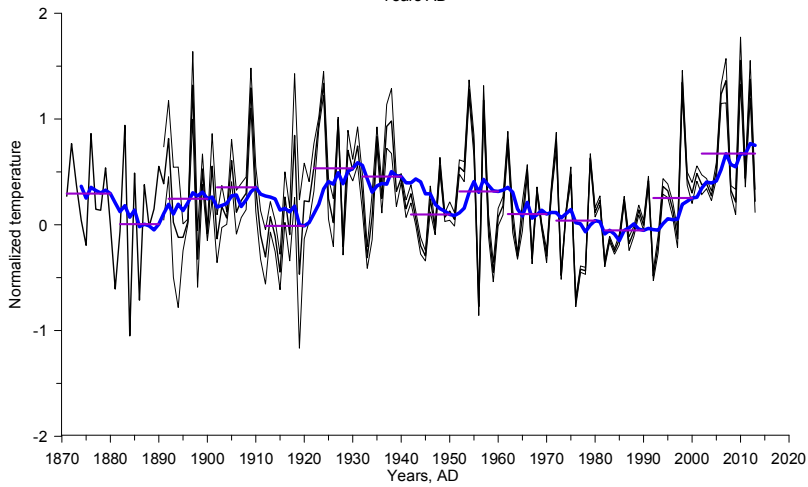


634  
635  
636  
637  
638

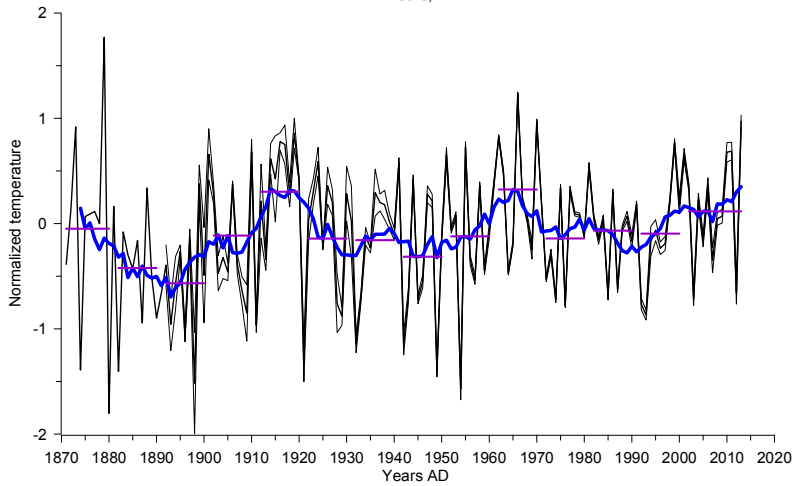
Fig. 7: Monthly  $\delta^{18}\text{O}$  (blue line),  $d$  (green line) and air temperature (red line) data at Bakuriani GNIP station in 2009 (see Table 1 for information on station and Fig. 1 for its location). Note that there is no clear seasonal cycle in deuterium excess, in contrast with  $\delta^{18}\text{O}$  showing maximum values in summer and minimum values in winter.



639



640



641

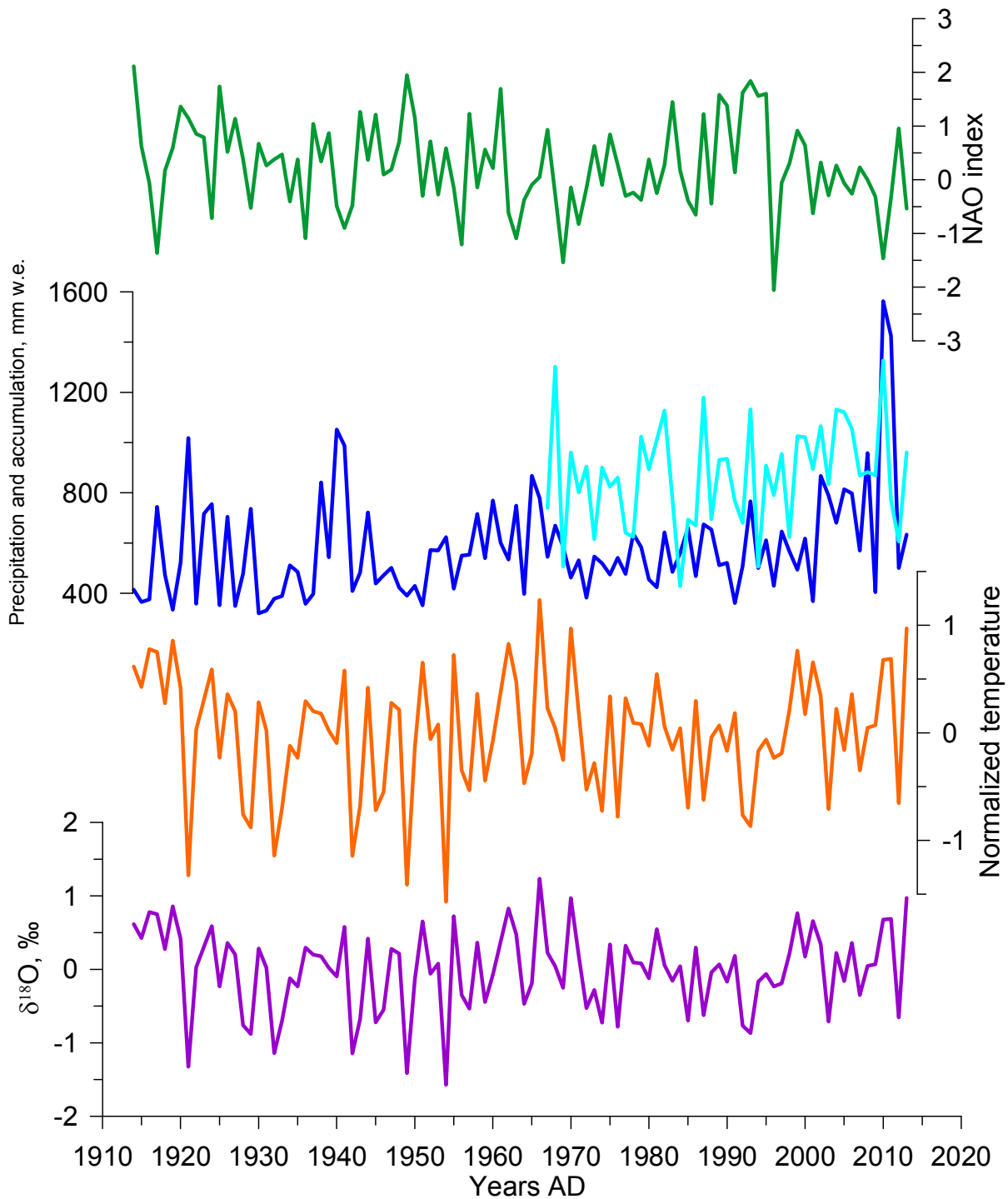
642

643

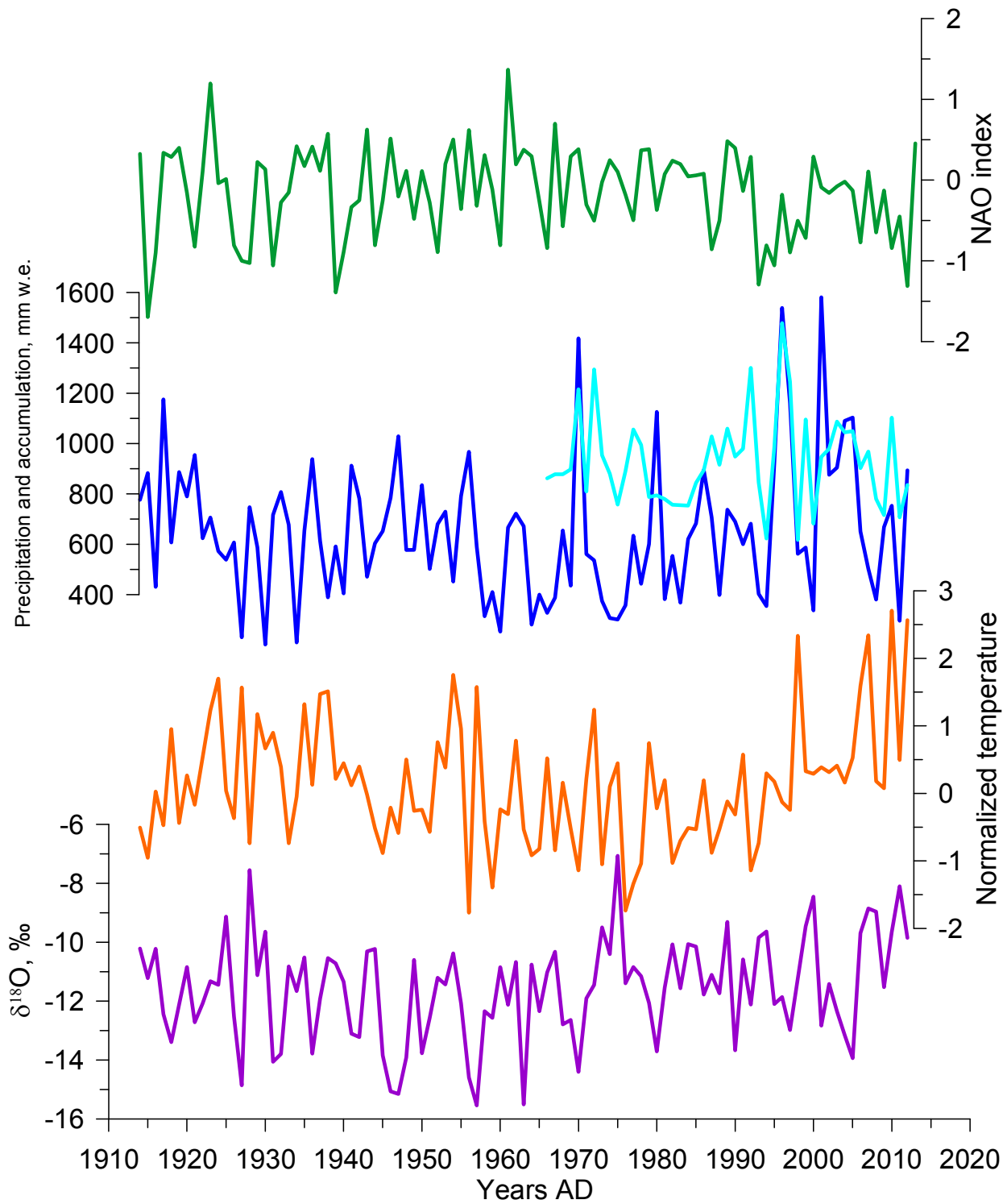
644

645

**Fig. 8: Normalized regional temperature record based on meteorological data, with respect to the reference period 1966-1990, expressed as annual anomalies (°C). The thin lines illustrate the standard deviation across the individual records after accounting for the lapse rate from Fig. S3, the blue line shows 10 year running mean and the horizontal purple line demonstrates the decadal mean value, the upper panel for the annual means, middle panel for the warm season, and the lower panel for the cold season.**



646  
 647 **Fig. 9: Comparison of the ice core record with instrumental regional climate information, for the cold season:  $\delta^{18}\text{O}$  composite**  
 648 **(purple), temperature at the drilling site calculated from the lapse rate (brown), precipitation at the Klukhorskii Pereval station**  
 649 **(light blue) as well as the ice core accumulation estimate (dark blue) and NAO index(green).**  
 650



651  
 652  
 653

Fig. 10: Same as fig. 9 but for the warm season.

654 **Table 1: Description of meteorological and instrumental data used in the paper**

Data type	Number on map (Fig. 1)	Location/Name	Altitude a.s.l.	Time span	Data source		
Meteorological observations (temperature, precipitation rate) with daily resolution	1	Sochi	57 m	1871-present	www.meteo.ru		
	2	Mineralnye Vody	315 m	1938-present			
	3	Kislovodsk	943 m	1940-present			
	4	Pyatigorsk	538 m	1891-1997			
	5	Shadzhatmaz	2070 m	1959-present			
	6	Terskol	2133 m	1951-2005			
	7	Klukhorskiy Pereval	2037 m	1959-present			
	8	Teberda	1550 m	1956-2005			
	9	Sukhumi	75 m	1904-1988			
	10	Samtredia	24 m	1936-1992			
	13	Tbilisi	448 m	1881-1992			
	14	Sulak	2927 m	1930-present			
	15	Mestia	1417 m	1930-1991			
	GNIP data	11	Batumi	32 m		1980-1990	<a href="http://www-naweb.iaea.org/napc/ih/IHS_resources_gnip.html">http://www-naweb.iaea.org/napc/ih/IHS_resources_gnip.html</a>
		12	Bakuriani	1700 m		2008-2009	
13		Tbilisi	448 m	2008-2009			
Circulation indices	n/a	NAO	n/a	1821-present	Vinter et al., 2009 <a href="https://crudata.uea.ac.uk/~timo/datasets/naoi.htm">https://crudata.uea.ac.uk/~timo/datasets/naoi.htm</a> <a href="http://www.cpc.ncep.noaa.gov/products/precip/CWlink/">http://www.cpc.ncep.noaa.gov/products/precip/CWlink/</a>		
			n/a	1950-present			
	n/a	NCP	n/a	1948-present			
	n/a	AO	n/a	1950-present			
Reanalysis daily temperature	n/a	NCEP	500 mb level	1948-present	<a href="http://www.esrl.noaa.gov/psd/data/gridded/data.ncep.reanalysis.html">http://www.esrl.noaa.gov/psd/data/gridded/data.ncep.reanalysis.html</a> Kalnay et al., 1996		
Back trajectories	n/a	Flexpart	n/a	2002-2009	Forster et al., 2007, Stohl et al., 2009		
	n/a	Hysplit	n/a	1948-present	Draxler, 1999, Stein et al., 2015, Rolph, 2016		
	n/a	LMDZiso	n/a	n/a	Risi et al., 2010		

655

656  
657  
658  
659  
660

**Table 2: Correlation coefficients between meteorological data and indices of large-scale modes of variability (statistically significant coefficients at  $p < 0.05$  are highlighted in bold). The period of calculation and number of data points (n) for each coefficient are shown in brackets.**

Annual mean	Temperature	P south*	P north*
NAO	<b>-0.24</b> (1914-2013, n=100)	-0.24 (1966-2013, n=48)	-0.03 (1966-2013, n=48)
AO	<b>-0.34</b> (1950-2013, n=64)	-0.06 (1966-2013, n=48)	0.02 (1966-2013, n=48)
NCP	<b>-0.55</b> (1948-2013, n=66)	0.26 (1966-2013, n=48)	0.26 (1966-2013, n=48)
Warm season			
NAO	<b>-0.47</b> (1914-2013, n=100)	0.23 (1966-2013, n=48)	0.03 (1966-2013, n=48)
AO	-0.11 (1950-2013, n=64)	0.08 (1966-2013, n=48)	0.14 (1966-2013, n=48)
NCP	<b>-0.50</b> (1948-2013, n=66)	<b>0.34</b> (1966-2013, n=48)	<b>0.34</b> (1966-2013, n=48)
Cold season			
NAO	<b>-0.41</b> (1914-2013, n=100)	0.04 (1966-2013, n=48)	0.26 (1966-2013, n=48)
AO	<b>-0.40</b> (1950-2013, n=64)	0.14 (1966-2013, n=48)	<b>0.37</b> (1966-2013, n=48)
NCP	<b>-0.77</b> (1948-2013, n=66)	0.25 (1966-2013, n=48)	<b>0.33</b> (1966-2013, n=48)

661  
662  
663  
664  
665  
666  
667

\*P south – precipitation rate at the weather stations to the South from the Caucasus, P north – precipitation rate at the weather stations to the North from the Caucasus.

668

**Table 3: Mean characteristics of the Elbrus ice core records, calculated for the period from 1914 to 2013.**

<b>Annual means</b>	$\delta^{18}\text{O}$ , ‰	$\delta\text{D}$ , ‰	$d$ , ‰	Accumulation rate (m w.e./year)
Mean	-15.90	-110.10	17.11	1,29
Standard deviation	1.76	14.03	1.02	0.44
<b>Cold season</b>				
Mean	-19.61	--140.11	16.59	0.71
Standard deviation	2.81	22.54	2.11	0.36
<b>Warm season</b>				
Mean	-11.58	-75.97	16.69	0.65
Standard deviation	1.75	13.98	1.14	0.27

669  
670

671  
672  
673

**Table 4. Correlation coefficients between ice core data, meteorological data and indices of large-scale modes of variability (statistically significant coefficients at  $p < 0.05$  are highlighted in bold). The period of calculation and number of data points (n) for each coefficient is shown in brackets.**

Annual means	$\delta^{18}\text{O}$	Accumulation	$d$	NAO	AO	NCP
$T$ , °C	-0.01 (1914-2013, n=100)	<b>0.16</b> (1914-2013, n=100)	0.00 (1914-2013, n=100)	<b>-0.24</b> (1914-2013, n=100)	<b>-0.34</b> (1950-2013, n=64)	<b>-0.55</b> (1948-2013, n=66)
P north*	<b>-0.30</b> (1966-2013, n=48)	<b>0.36</b> (1966-2013, n=48)	0.17 (1966-2013, n=48)	-0.03 (1966-2013, n=48)	-0.03 (1966-2013, n=48)	0.27 (1966-2013, n=48)
P south*	0.06 (1966-2013, n=48)	<b>0.52</b> (1966-2013, n=48)	0.07 (1966-2013, n=48)	-0.24 (1966-2013, n=48)	-0.06 (1966-2013, n=48)	0.18 (1966-2013, n=48)
$\delta^{18}\text{O}$		<b>-0.20</b> (1914-2013, n=100)	-0.06 (1914-2013, n=100)	0.07 (1914-2013, n=100)	<b>0.41</b> (1950-2013, n=64)	0.11 (1948-2013, n=66)
Accumulation			<b>0.21</b> (1914-2013, n=100)	<b>-0.29</b> (1914-2013, n=100)	<b>-0.29</b> (1950-2013, n=64)	-0.03 (1948-2013, n=66)
$d$				-0.08 (1914-2013, n=100)	<b>-0.26</b> (1950-2013, n=64)	-0.14 (1948-2013, n=66)
Warm season	$\delta^{18}\text{O}$	Accumulation	$d$	NAO	AO	NCP
$T$ , °C	0.13 (1914-2013, n=100)	-0.04 (1914-2013, n=100)	<b>0.20</b> (1914-2013, n=100)	-0.02 (1914-2013, n=100)	-0.10 (1950-2013, n=64)	<b>-0.51</b> (1948-2013, n=66)
P north*	0.01 (1966-2013, n=48)	0.16 (1966-2013, n=48)	0.09 (1966-2013, n=48)	0.13 (1966-2013, n=48)	-0.14 (1966-2013, n=48)	0.18 (1966-2013, n=48)
P south*	-0.27 (1966-2013, n=48)	<b>0.49</b> (1966-2013, n=48)	-0.02 (1966-2013, n=48)	-0.01 (1966-2013, n=48)	0.07 (1966-2013, n=48)	<b>0.34</b> (1966-2013, n=48)
$\delta^{18}\text{O}$		<b>-0.42</b> (1914-2013, n=100)	-0.05 (1914-2013, n=100)	-0.08 (1914-2013, n=100)	0.16 (1950-2013, n=64)	0.00 (1948-2013, n=66)
Accumulation			<b>0.31</b> (1914-2013, n=100)	0.00 (1914-2013, n=100)	0.09 (1950-2013, n=64)	0.00 (1948-2013, n=66)
$d$				0.00 (1914-2013, n=100)	-0.01 (1950-2013, n=64)	-0.14 (1948-2013, n=66)
Cold season	$\delta^{18}\text{O}$	Accumulation	$d$	NAO	AO	NCP
$T$ , °C	-0.09 (1914-2013, n=100)	0.11 (1914-2013, n=100)	-0.15 (1914-2013, n=100)	<b>-0.30</b> (1914-2013, n=100)	<b>-0.45</b> (1950-2013, n=64)	<b>-0.79</b> (1948-2013, n=66)
P north*	0.20 (1966-2013, n=48)	0.21 (1966-2013, n=48)	-0.12 (1966-2013, n=48)	<b>0.51</b> (1966-2013, n=48)	<b>0.37</b> (1966-2013, n=48)	0.23 (1966-2013, n=48)
P south*	<b>-0.30</b> (1966-2013, n=48)	<b>0.37</b> (1966-2013, n=48)	-0.13 (1966-2013, n=48)	0.26 (1966-2013, n=48)	0.14 (1966-2013, n=48)	0.25 (1966-2013, n=48)
$\delta^{18}\text{O}$		0.05 (1914-2013, n=100)	0.02 (1914-2013, n=100)	<b>0.41</b> (1914-2013, n=100)	<b>0.41</b> (1950-2013, n=64)	0.19 (1948-2013, n=66)
Accumulation			0.07 (1914-2013, n=100)	-0.18 (1914-2013, n=100)	-0.15 (1950-2013, n=64)	0.18 (1948-2013, n=66)
$d$				-0.06 (1914-2013, n=100)	-0.01 (1950-2013, n=64)	0.11 (1948-2013, n=66)

\*P south – precipitation rate at the weather stations to the South from the Caucasus, P north – precipitation rate at the weather stations to the North from the Caucasus.

674  
675